Development of nanoparticle catalysts and total internal reflection (TIR) Raman spectroscopy for improved understanding of heterogeneous catalysis

LAURA MARIA BINGHAM

Chapter 2. Methodology and experimental

2.1. Methodology

2.1.1. Transmission electron microscopy (TEM)

In TEM the interaction of electrons (emitted from the electron gun) with the chosen sample and subsequent collection of transmitted electrons allow imaging to take place. The diffraction and Energy Dispersive X-ray (EDX) spectroscopy modes of the TEM allow for determination of crystal structure and sample composition respectively. A schematic of the design of a conventional electron microscope is shown in Figure 2.1. The microscope works by first emitting electrons from the electron gun, typically by thermionic (heat induced) emission. The electrons are then focused onto the sample using as series of condensers (a two stage system is shown in Figure 2.1). This allows for control of the sample area illuminated. The electrons which hit the sample interact and lead to electron scattering (elastic or inelastic) or absorption, which may in turn lead to fluorescence or photoelectron emission. The lens collects the number density of electrons that pass through the sample without interaction. A lens system is then used to produce an image of the electron density distribution. The image can either be formed by electrons interacting with a phosphor screen for observation in real time or then recorded, traditionally using a photographical emulsion, but more recently by use of a charge-coupled device (CCD) camera. A small objective lens aperture is needed to provide well resolved images. Bright field (BF) contrast comes from electrons scattered through larger angles than the objective lens aperture.

A thin sample is needed, due to the strong elastic and inelastic interactions of electrons with atoms. The mean free path of an electron is short (relative to that of a photon), and so fewer electrons will pass through a thick sample.[1]

X-rays emitted after electronic excitation of the sample by electrons can be collected for EDX chemical analysis. Absorption of the X-rays in the detector leads to the creation of high-energy photoelectrons which in turn lead to the production of charge carriers. For example in semiconductors charge carriers result from the creation of electron-hole pairs. The number of charge carriers is proportional to the X-ray quantum energy (as expressed by $E_{X\text{-}ray} = h\nu$), therefore by measuring the pulse height the number of X-rays hitting the detector can be calculated.[1]

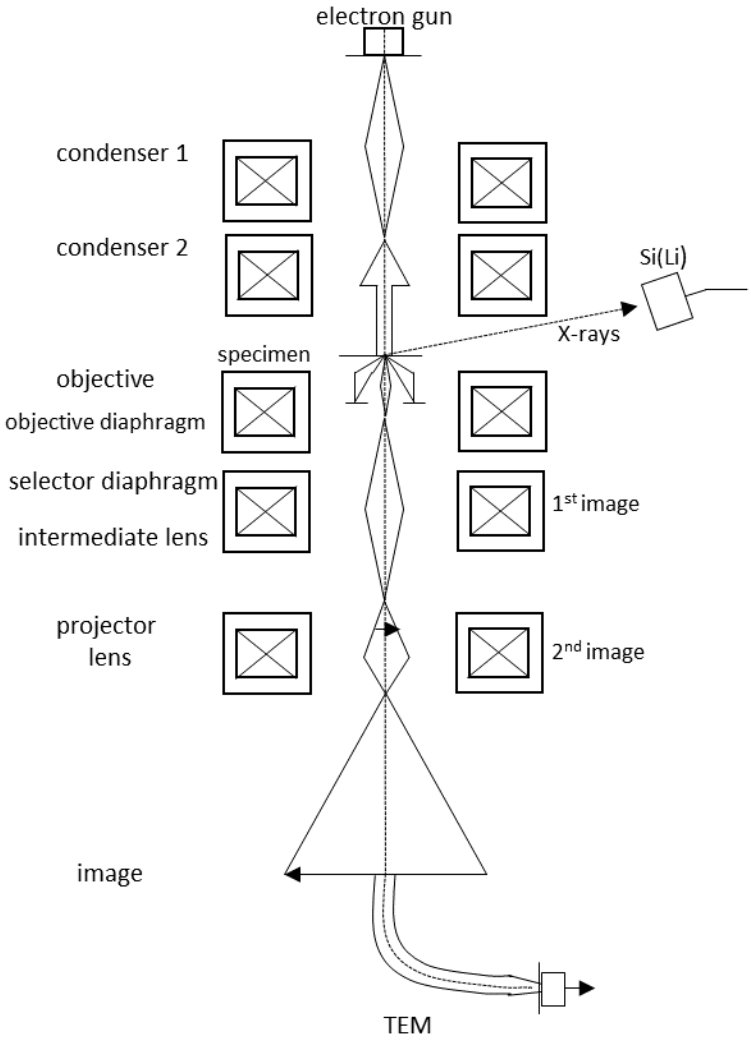

Figure 2.1. Diagram adapted from Reimer et al.,[1] showing a conventional electron microscope, including the ray path, for a system fitted with X-ray and electron energy loss spectroscopy.

2.1.2. Scanning electron microscopy (SEM)

SEM shares a number of similarities with TEM, with the main difference being that in SEM the electrons are scattered rather than transmitted. When the electron current hits the sample it is deflected rather than focused through the lens for imaging. As the electron beam scans across the surface (not the internal sample as in TEM) changes in composition, texture, and topography are recorded. These changes cause variation in the electron current and so are present in the image observed.[2] It should be noted that as it is the surface being scanned any thickness of sample can be used.

2.1.3. X-ray photoelectron spectroscopy (XPS)

XPS is a surface sensitive technique allowing for chemical analysis. The technique takes its roots from the photoelectric effect as shown in Figure 2.2.[3,4] X-rays are used to excite a core level electron in an atom located at/just below the surface of the sample. This leads to

ejection of this photoelectron. The kinetic energy E_{kin} of the ejected electron can be related, *via* the conservation of energy, to the initial energy *h*v, the work function Φ, and the change in energy of the sample upon losing the core electron E_b as shown in Figure 2.2 and Equation 2.1. The binding energy E_b is an important term since it shows how tightly bound an electron is within the atom. XP spectra are conventionally plotted against binding energy on the x axis.

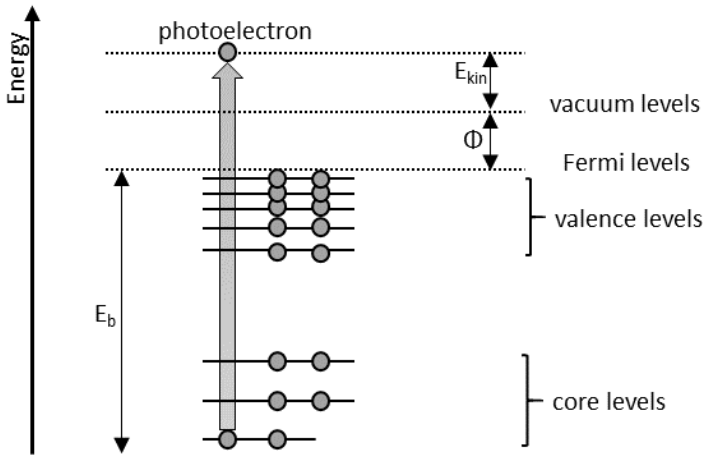

Figure 2.2. Diagram to show X-ray photoemission process.

$$E_{kin} = h\nu - E_b - \Phi \qquad \textit{Equation 2.1}$$

The electrons being ejected from the surface atoms are then filtered by their energy using a hemispherical analyser (HSA).[5] A detector then records the intensity for this set energy. The quantised nature of the core level electrons means the energy spectrum obtained has peaks that are characteristic of the electronic structure of the atoms probed, and element specific. Since the spectral peak position is determined by the electronic state of the atom the chemical environment surrounding the surface atom (such as oxidation of the element) results in changes in the characteristic binding energy of the peak.[5]

2.1.3.1. Quantification

XPS is well suited to quantification as the signal intensity is related to three key factors: the concentration of the species at the sample surface, the probability of excitation from that core level, and the probability of the photoelectron escaping the surface (without undergoing an inelastic collision). Quantification can take place as the third factor can be ignored if the concentration of surface adsorbates is low and only a few surface atomic layers are of interest, and the second factor can be corrected by taking into account the

photoionisation cross section (tabulated values which were in our case in built into the software package used for analysing the XP spectra).

2.1.3.2. Background fitting

Background removal took place using a Shirley background, chosen as it is one of the most commonly used fittings and compensates for the inelastic scattering background. In cases not applicable to fitting of a Shirley background (*e.g. Chapter 3,* Section 3.2.1.2, Figure 3.15 B) a linear background was fitted.

2.1.4. Ultraviolet-visible (UV-vis) spectroscopy

The absorption of electromagnetic radiation in the visible and UV range leads to the creation of a UV-visible (UV-vis) spectra. This absorption spectrum is due to the excitation of the species (often a gas or liquid) to a higher electronic energy level. The frequency of such an absorption will be dependent upon the energy in that transition (*i.e.* the energy gap between the ground and excited state). Whilst the intensity of the peak depends upon the likelihood of the transition taking place, which is determined by selection rules. The absorbance is defined by the relation given in Equation 2.2.[6]

$$A = log(\frac{I_0}{I}) \qquad \textit{Equation 2.2}$$

Equation 2.2 shows the dependence of absorbance on the incident and measured intensity, where A=absorbance, I=measured intensity, I_0=incident intensity. For example if the measured intensity reduces by 1/10 of the incident (*i.e*. I_0=100 I=90) an absorbance of 0.046 would be recorded.

In this work UV-vis spectroscopy has been used to help determine if samples exposed to a particular wavelength laser, for Raman excitation, may also exhibit fluorescence, since samples that do not absorb significantly at a given wavelength should not fluoresce. This is because in the UV-vis spectroscopic experiment absorbed photons cause electronic excitation to higher energy states. Relaxation can then take place by fluorescence, non-radiative relaxation, or a mixture of the two. Although there is no guarantee that if UV-vis absorbance is detected that fluorescence should also occur, the converse situation when no absorbance occurs (and so no fluorescence can occur) is useful in narrowing down the most appropriate samples to study and most appropriate wavelength to study them with.

2.1.4.1. UV-visible (UV-vis) spectroscopy for the elucidation of surface plasmon absorbance bands in metal nanoparticles

Surface plasmon resonance in metal nanoparticles, which is associated with the oscillation of electrons in a surface with a wavelike energy, results from the movement of free electrons through a metal.[7] The band seen will depend upon the particles' shapes and sizes as well as the nature of the chemical surroundings including the solvent medium.[8–11] This coincides with the distinct colours typically seen for nanoparticle solutions. The colour is often used as a crude indication of particle size.[12–15]

In the same way that the progress of the reaction can be monitored by observing the solution's colour change, the presence of surface plasmon absorbance bands can be followed using UV-vis spectroscopy. The position and shape of the plasmon absorption for metal nanoparticles is known to be strongly dependent on the particle size. However, there are several disadvantages to such use of this technique. UV-vis spectroscopy is an indicator of particle size, but this can be difficult to take advantage of given a number of factors. For example the particle size detected may be altered by other variables such as the choice of capping agent used. Furthermore the value obtained is only an average and only nanoparticles of a certain size range will be detected. So very small or large particles present avoid detection leading to false assumptions about the particles size and distribution. As a result, other techniques such as TEM, powder X-ray diffraction (PXRD) and extended X-ray absorption fine structure (EXAFS) spectroscopy are more widely used to assess or confirm nanoparticle size.

2.1.5. Raman spectroscopy underlying theory and practical considerations

2.1.5.1. Theory

Raman scattering is the inelastic scattering of a single photon leading to a transition between vibrational or rotational energy levels.[16] Raman scattering occurs when a photon interacts with a molecule, causing an excitation to a short lived virtual state (given by vibrational levels in Figure 2.3). Relaxation then occurs releasing energy, in the form of a photon, which is recorded in Raman spectra. The energy change between final and initial state can give rise to Stokes or anti-Stokes lines. When no net energy change occurs Rayleigh lines are observed. For Stokes lines excitation occurs from the ground state (v=0) to the virtual level, and a photon is given out on relaxation to a vibrationally excited state (*e.g.* v=1). The energy released is less than the excitation energy put in. This is the most common occurrence, especially for vibrational transitions where only the v=0 state is significantly populated near

ambient temperature. Anti-Stokes excitation occurs from a vibrationally excited state to a lower energy vibrational energy level (*e.g.* v=0), relaxation gives out a photon of greater energy than that which caused the excitation.[17] These three processes are shown in Figure 2.3. The Stokes process occurs at longer wavelengths *i.e.* lower energy.

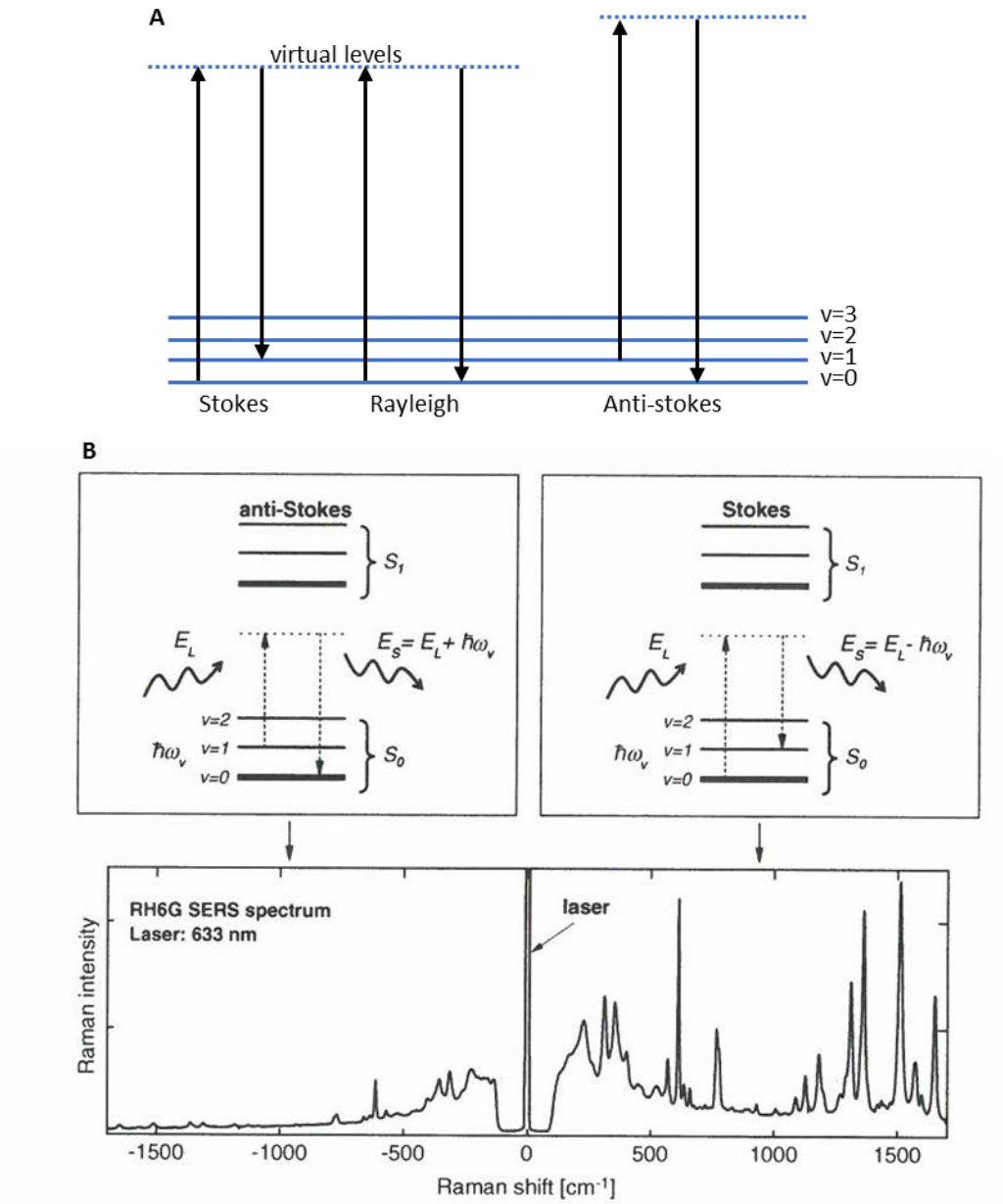

Figure 2.3. A) A diagram showing the electronic transitions caused by excitation in a molecule via a photon, and the subsequent stokes, anti-stokes and Rayleigh lines present in resulting spectra. The diagram was adapted from Gardiner and Graves,[17] B) Jablonski diagram and an exemplar Raman spectra to exemplify stokes and anti-stokes Raman processes reproduced from Principles of Surface-Enhanced Raman Spectroscopy (without being able to obtain permission).[18] Where E_L = the incident photon energy, E_s = scattered photon energy, h = planks constant, w_v = frequency for transition between vibrational states, S_0 = ground vibrational structure for vibrational states v=0, 1, 2. S_1 = excited vibrational substructure.

2.1.5.2. Selection rules: gross and specific for vibrational Raman with comparison to infrared (IR) spectroscopy

Selection rules can be categorised as gross or specific, where gross selection rules indicate the general features required in a molecule for a spectrum of any kind to be recorded.[19] Specific selection rules provide the allowed transitions in terms of changes in quantum

numbers.[19] The gross selection rule for vibrational Raman spectroscopy specifies that a change in polarisability must take place as the molecule vibrates. In contrast, for IR the selection rule, for both rotational and vibrational spectroscopy, requires that a change in dipole moment must take place. For both IR and Raman vibrational spectroscopy the specific selection rule is that $\Delta v=\pm 1$, where v is the quantum number.

2.1.5.2.1. Diatomics and polyatomics

As a consequence of the gross selection rule both homonuclear and heteronuclear diatomics are Raman active. The application of selection rules for polyatomics is in general more complex due to the variety of different vibrational modes available. In order to express this we can first start by calculating the number of normal modes, or independent modes, available for a given molecule. This is given by 3N-6, or 3N-5 for a linear molecule, where N is the number of atoms present. For example in water we would have N=3, giving a total of 3 normal modes. At this point we can then further categorise these modes according to the nature of the vibration *e.g.* symmetric, and asymmetric stretching, and bending modes. We can then deduce if these normal modes in the polyatomic will be active for Raman vibrational or IR spectroscopy, although group theory is often required to determine if a modes will be active particularly for large complex molecules. However, in many cases simple inspection of the mode can be sufficient. One general rule for a (diatomic or polyatomic) molecule is that of mutual exclusion which states that a molecule which has a centre of symmetry cannot have any modes which are both IR and Raman active. In IR spectroscopy a normal mode will be active if a change in dipole moment takes place. In a simple molecule like carbon dioxide we can see that the asymmetrical stretch results in the molecule becoming unsymmetrical. This results in a change in dipole moment making this mode IR active. However, for the symmetrical mode no asymmetry takes place for this mode and so no change in dipole moment is seen therefore this mode is IR inactive. In Raman vibrational spectroscopy a normal mode will be active if a change in polarisability is seen.[19] It can often be difficult to deduce if a mode will be Raman active, but one simple example is again given by carbon dioxide. In carbon dioxide the symmetrical stretch results in the molecule swelling and contracting which results in a change in polarisability making this mode allowed. No change in polarisability is seen for any of the other normal modes in carbon dioxide.[19]

2.1.5.3. Practical considerations: potential advantages and disadvantages of Raman spectroscopy in comparison to other in situ techniques

Raman spectrometers contain a laser which emits single frequency excitation radiation. The spectrometer then detects the emission that follows the excitation. In contrast to IR spectroscopy this excitation can use visible radiation meaning that glass optics can be used. Other differences between Raman and IR spectroscopy include the selection rule requirements. For IR spectroscopy molecules must have a change in dipole moment, this is not required for Raman spectroscopy where a change in polarisability is instead required. Raman spectroscopy therefore offers advantages over IR in the detection of molecules which are not IR active (*i.e.* homonuclear diatomics). Furthermore, water and carbon dioxide are both weak Raman scatterers meaning that, unlike in IR spectroscopy, no purging of samples is required. This is important in catalysis where water is often a product or solvent. Other advantages of Raman spectroscopy include its operation over wide temperature and pressure ranges (-273 to >1000 °C, and 10^{-7} to >10^{6} Pa) as well as its ability to provide molecular level information.[20]

However, there are several disadvantages for Raman spectroscopy. The most considerable being its low sensitivity, compared to techniques such as IR spectroscopy. For example, typical photon cross sections for Raman and IR spectroscopic processes differ by around 6 orders of magnitude (typical values are Raman $\sigma \sim 10^{-29}$ m^2, IR $\sigma \sim 10^{-23}$ m^2).[21] To overcome low sensitivity, intense laser beams can be used. This improves the number of Raman scattered photons, but can, however, cause irreversible sample damage.[22,23] Indeed samples studied by Raman spectroscopy can be prone to decomposition due to localised heating. One possible solution is to place the sample on a spinning disk which reduces the amount of time the beam remains in one area resulting in reduced sample damage. Another potential disadvantage of Raman spectroscopy is fluorescence. Samples which fluoresce give a strong signal that often obscures the weak Raman bands (see Chapter 3 for examples and discussion). Solutions have been offered to reduce this effect, and changing the laser wavelength can often help.[1,6] As discussed above UV-vis absorption spectroscopy can be a viable method of determining at which wavelengths fluorescence could occur.

2.1.5.4. Total internal reflection (TIR) Raman spectroscopy

In TIR Raman the spectroscopy occurs in the evanescent wave, in order to achieve this there are two conditions required to allow total internal reflection. Firstly, at least one side should be accessible to light, and, secondly, the refractive index of the first medium, the laser light

hits, should be higher than that of the second medium.[24] A schematic of a TIR Raman set-up is shown in Figure 2.4. As can be seen the polarised laser light (in this case a 532 nm laser beam) travels through the first medium (typically air) and then hits the hemisphere, the base of which is coated in a monolayer of the material to be studied. The majority of the incident laser light is then reflected through the hemisphere and is collected at the beam block (labelled power dissipation in Figure 2.4). The incident photons can interact with the sample as a result of the evanescent decay, and a small number of these incident photons undergo Raman scattering. The Raman scattered light is first collected by the objective lens, and then focussing lenses (tube lens and "eyepiece lens") image the photons from the sample on the slit entrance to the spectrograph. The Raman scattered light needs to be passed through a filter (in our case an edge filter) to remove the strong Rayleigh line, and can then, if desired, be filtered further to produce a single polarisation. Finally the light is dispersed according to wavelength, by diffraction gratings in the spectrograph, and detected on the CCD camera. The spectrograph results in the position of the camera being wavelength dependent, generating a spectrum of Raman scattered light. It should be noted the intensity of the Raman scattered light decays exponentially from the reflection interface because of the evanescent profile of the excitation light. This results in the signal obtained being constrained to the surface of the hemisphere. This constraint on the probing depth is greater than can be achieved through confocal microscopy alone. This is a desirable feature for studying a heterogeneous catalyst for which chemistry occurs at the catalyst surface, furthermore we are interested in discriminating this from the bulk reagents. Another key feature of this system is that the majority of the power is dissipated away from the surface being probed. This results in a reduced likelihood of laser induced sample damage, allowing for the use of higher powered lasers. This allows for enhancement in the sensitivity of TIR in practice in comparison to confocal Raman spectroscopy.

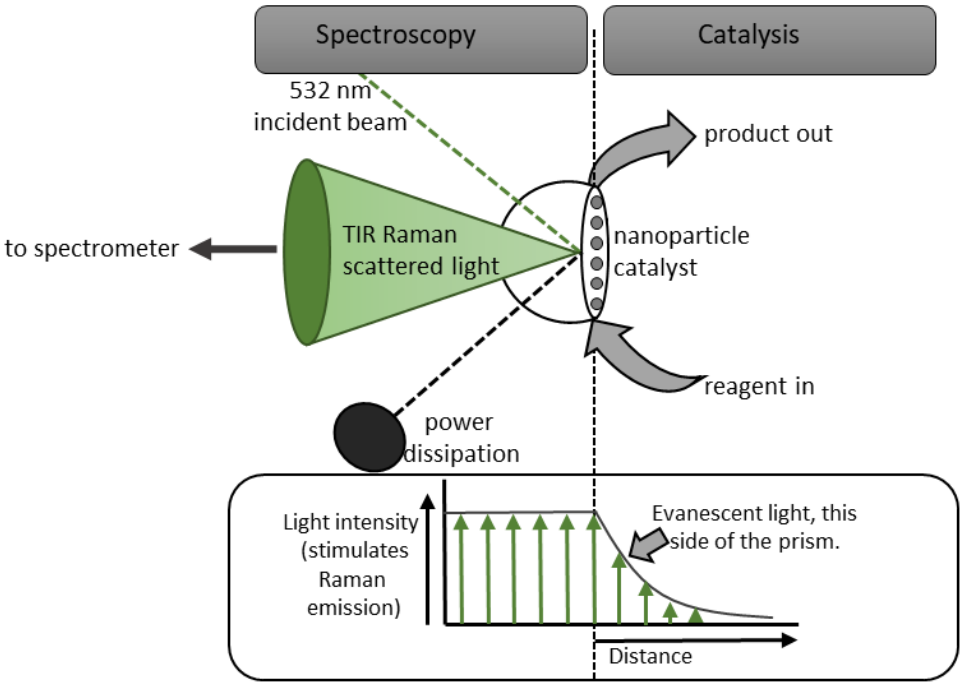

Figure 2.4. Schematic of typical TIR Raman set-up for the study of nanoparticle catalysts.

2.1.5.5. Fresnel coefficients and polarisation

For light reflected at a surface it is possible to calculate the intensity of different polarized components using Fresnel equations. The Fresnel equations can be derived, but for simplicity the following equations (Equations 2.3-2.5) are stated as sufficient for present consideration.

$$K_{p,x} = \frac{2n_i cos\theta_i cos\theta_t}{n_t cos\theta_i + n_i cos\theta_t} \qquad \textit{Equation 2.3}$$

$$K_{s,y} = \frac{2n_i cos\theta_i}{n_i cos\theta_i + n_t cos\theta_t} \qquad \textit{Equation 2.4}$$

$$K_{p,z} = \left(\frac{n_t}{n'}\right)^2 \frac{2n_i cos\theta_i sin\theta_t}{n_t cos\theta_i + n_i cos\theta_t} \qquad \textit{Equation 2.5}$$

These Equations 2.3 to 2.5 relate to coefficients below the critical angle, where n_i and n_t are the refractive index of the incident and transmitted materials, and θ_i and θ_t are the angle of incidence and refraction of the laser beam respectively. The critical angle is the angle of the laser light's incidence at which the greatest emitted signal is measured.[16] Fresnel factors relate the incident electric field to that which is reflected or refracted through the material. This is dependent upon the polarisation of the laser beam. The beams polarisation is defined relative to the direction at which the incident laser light propagates, and is categorised as either p or s, p being polarisation parallel and s perpendicular to the propagating laser light's electric field. Fresnel coefficients can be calculated for both s and p polarised light in the x, y, and z directions. Fresnel coefficients are therefore denoted by the terms $K_{p,x}$, $K_{s,y}$, and

$K_{p,z}$ referring to the coefficients in the with p or s polarisation in the x, y, or z directions. Finally the angle of refraction (θ_t) is given by Snell's law (Equation 2.6).

$$sin\theta_t = \left(\frac{n_i}{n_t}\right) sin\theta_i \quad \textit{Equation 2.6}$$

This will be discussed further in Chapter 5 in terms of incident laser angles chosen and their impact upon the number of free and absorbed gas molecules probed.

2.1.5.6. CCD, edge filter, and diffraction gratings: design and considerations for Raman spectroscopy

2.1.5.6.1. Edge filters

An edge filter is typically comprised of alternating layers of dielectric stacks and space layers with the filter cased within an aluminium ring (Figure 2.5).[25] Between each space layer and the dielectric stack is a space cavity (termed a Fabry-Perot cavity).[26] Constructive interference conditions within this cavity allows for the transmission of light at a central wavelength, and also low intensity regions of wavelength either side of this central value (*i.e.* a plot of transmission against wavelength is a bell curve with the majority of the transmission taking place at a wavelength within the central band in the middle of the bell curve). Correspondingly this type of filter is often characterised as having a region of low and high transmittance lying adjacent to one another.[27] This results in a filter that is efficient in working within a defined wavelength region. In order to reduce or eliminate altogether these areas of low transmission the substrate or space layer can be coated in a material which acts to block these wavelength regions. However, these coatings can also act to reduce transmission for the central band of interest.

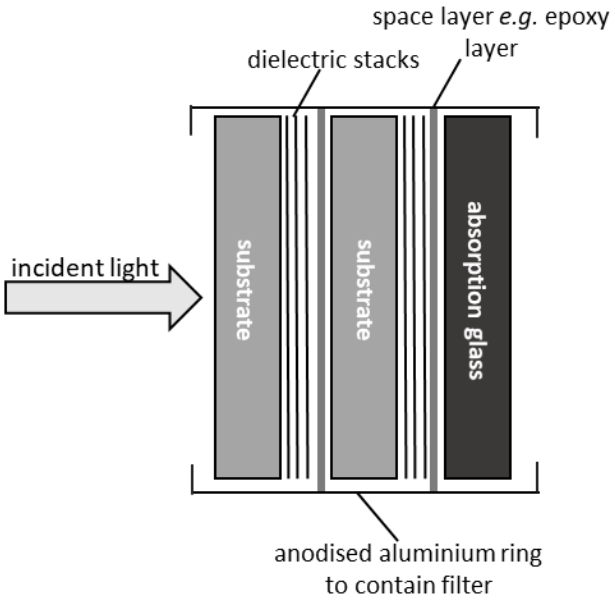

Figure 2.5. Schematic to show typical structure of an edge filter comprised of layers of dielectric stacks and space layers.

2.1.5.6.2. Diffraction gratings

A diffraction grating allows for the separation of light depending upon its wavelength. Two common types of diffraction grating are transmission and reflective.[19] In a transmission grating a repetitive structure of evenly spaced etches are used to scatter the incident light (Figure 2.6, A). A reflective grating is comprised of a reflective coating (such as a metal, epoxy or plastic) deposited upon the optic onto which parallel grooves are then scored. Light then reflects off the surface at differing angles depending upon its wavelength (Figure 2.6,B).[28] The latter sort is commonly used in optical spectrographs and was used in all systems in this work. Grating equations showing the relation between the incident and final angle (θ_i, and θ_m respectively) for light of a given wavelength are shown for both types of grating (Figure 2.6, A and B). From these equations it can be seen that the structure of the diffraction grating influences the properties of the light wave in terms of amplitude of phase, and more generally that light of differing wavelengths will exit the grating at different angles. It can be noted that for the reflective grating under certain conditions (where $\theta_i = \theta_m$) no wavelength dependency is seen meaning all light is lost and is either reflected or transmitted at the surface. However, this can be overcome for example through the use of a blazed (or ruled) grating where a repeating surface pattern is used to strategically alter the geometry of the surface reflection.

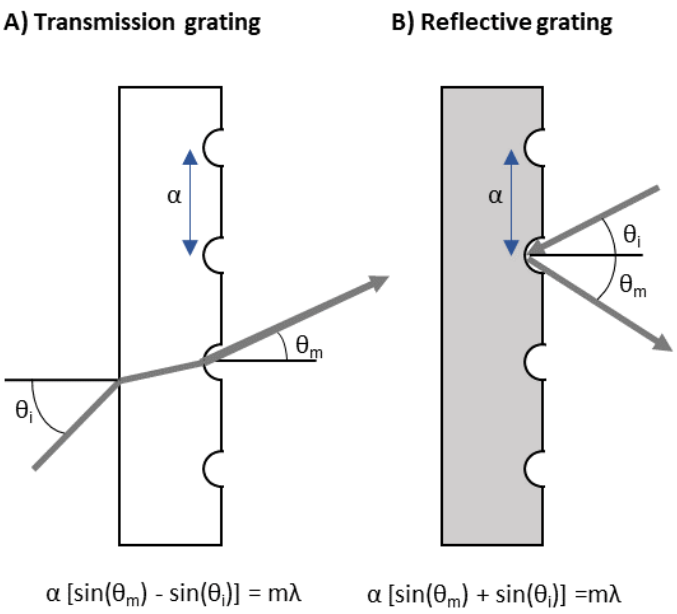

Figure 2.6. Diagrams, adapted from Thorlabs,[28] to show the path of light (with wavelength λ, entering at incident angle ϑ_i, and leaving at angle ϑ_m, where m is the order of principal maxima) through A) a transmission and B) a reflective diffraction grating (in both cases having a grating width α). Grating equations are given for both of the gratings shown.

2.1.5.6.3. CCD

The CCD is a 2-dimensional system compromised of several million individual photodiode detectors.[19] The CCD records the intensity of the light entering it. In order to allow for the Raman scattering from one wavelength of interest to be detected (*e.g.* for a feature of interest) this wavelength is passed through the spectrometer onto the CCD and the distribution for this feature is displayed.[17] Typically, spectra are acquired by binning columns of pixels perpendicular to the direction that the diffracted light has been spread in – many modern cameras can do this electronically within the CCD electronics to enable faster readout times.

2.1.6. Langmuir Blodgett (LB) deposition techniques

Monolayers can be defined as "surface films which are one layer thick".[19] Monolayers of molecular or colloidal materials can be prepared using a Langmuir Blodgett (LB) method where the sample is floated on a liquid surface and then transferred onto a solid material. When a monolayer is transported to a solid support it is called a LB film. A schematic of the apparatus used to achieve this (Figure 2.7) and an overview of the process leading to LB film formation (Figure 2.8) are both given below. The trough is first filled with water. A substrate can then be submerged into the water *via* lowering of the dipping axis, which is attached to the sample jaw (Figure 2.7). During this process material is dissolved in a suitable volatile

solvent that is immiscible with water, then placed upon the surface of the water already filling the trough. The substrate is subsequently pulled up out of the water, again *via* movement of the vertical dipping axis. During this process the surface monolayer adheres to the substrate giving a monolayer coating. In order to ensure that a surface monolayer is present, rather than multilayers or greater, careful selection of the surface pressure must take place for the deposited material upon the trough.

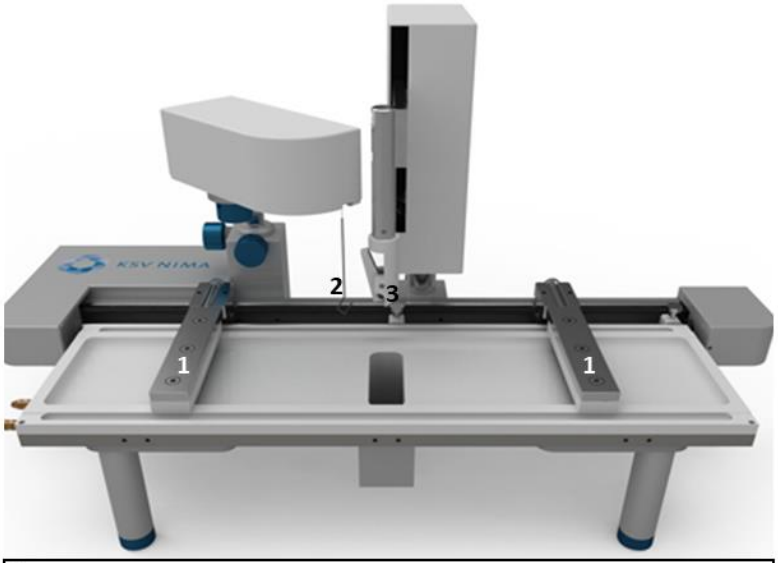

Key

1- trough barriers

2- Wilhelmy plate (for measuring surface pressure) hangs upon the metal hook

3- sample jaw on vertical axis

Figure 2.7. LB trough, image taken from manufacturer website, www.ksvnima.com

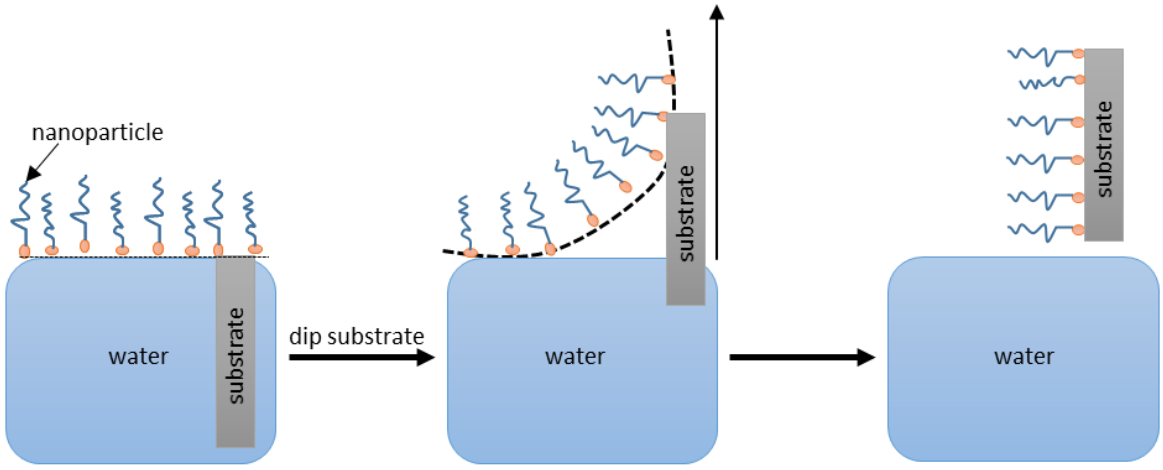

Figure 2.8. Diagram to show the process involved in LB film formation

2.1.6.1. Studying surface pressure with the LB trough

As mentioned above it is important to monitor the surface pressure on the LB trough. Primarily this is to provide a surface monolayer in order to allow for the monolayer coating of substrates. Furthermore the technique is also capable of providing a variety of information including: the area that the molecules occupy when in a closely packed arrangement, and an idea of the efficiency and tightness of molecular packing. In order to achieve the preparation of a surface monolayer the standard preparation procedure described above was used. The surface pressure was measured using a platinum plate, known as a Wilhelmy plate, resting upon the surface of the monolayer. It should be noted that in order to reduce solid liquid interactions between the water phase and the trough, the trough was coated in a hydrophobic material (typically PTFE).[19] An example of this compression process while monitoring surface pressure, for the case of platinum/ polyvinylpyrrolidone nanoparticles (Pt/PVP nps), is given in Figure 2.9. The right hand region of the curve (start of experiment – note time goes from right to left) shows surface pressure increasing as the barriers are closed (*i.e.* as the trough area decreases). This was expected as the nanoparticles now have less space to occupy, pushing the capping agents closer together. This makes the sterics less favourable, and so more energy is needed for compression and a higher surface pressure results. Also, with a higher quantity of molecules in the same area, the likelihood of collision increases and again this leads to an increased surface pressure. Then at a certain surface pressure the energy required for the molecules to stay in their current arrangement (*i.e.* side by side) becomes too high. Instead the particles form layers that slip over each other, decreasing the likelihood of collision and giving more favourable sterics (Figure 2.9). The more effective spacing of the particles results in a reduction in the variation of the surface pressure. This particle packing is referred to as multilayer formation. In this multilayer regime the surface pressure should not fluctuate significantly, as positions within each layer will not change (although the number of layers may). So the force the molecules exert upon each other also remains roughly constant. This results in a plateau being seen for a plot of surface pressure against surface area. This is characteristic of regions in which multilayers exist. Therefore, in order to create a surface monolayer the sample must be dipped at a surface pressure value below that at which this plateau occurs. For example in Figure 2.9 this would equate to surface pressure below 35 mN m^{-1}. In this case a value of 30 mN m^{-1} might be chosen as it would be expected to result in a tightly packed substrate surface. A tightly packed surface is not only desirable for the increased surface uniformity but also for the increased surface coverage provided. Both of these properties are advantageous when

producing a material for study using TIR Raman. Finally if calculation of the area the molecules occupy is required this is gained by simply extrapolating the steepest part of a curve of surface pressure against molecular area, as this relates to a monolayer closely packed region.

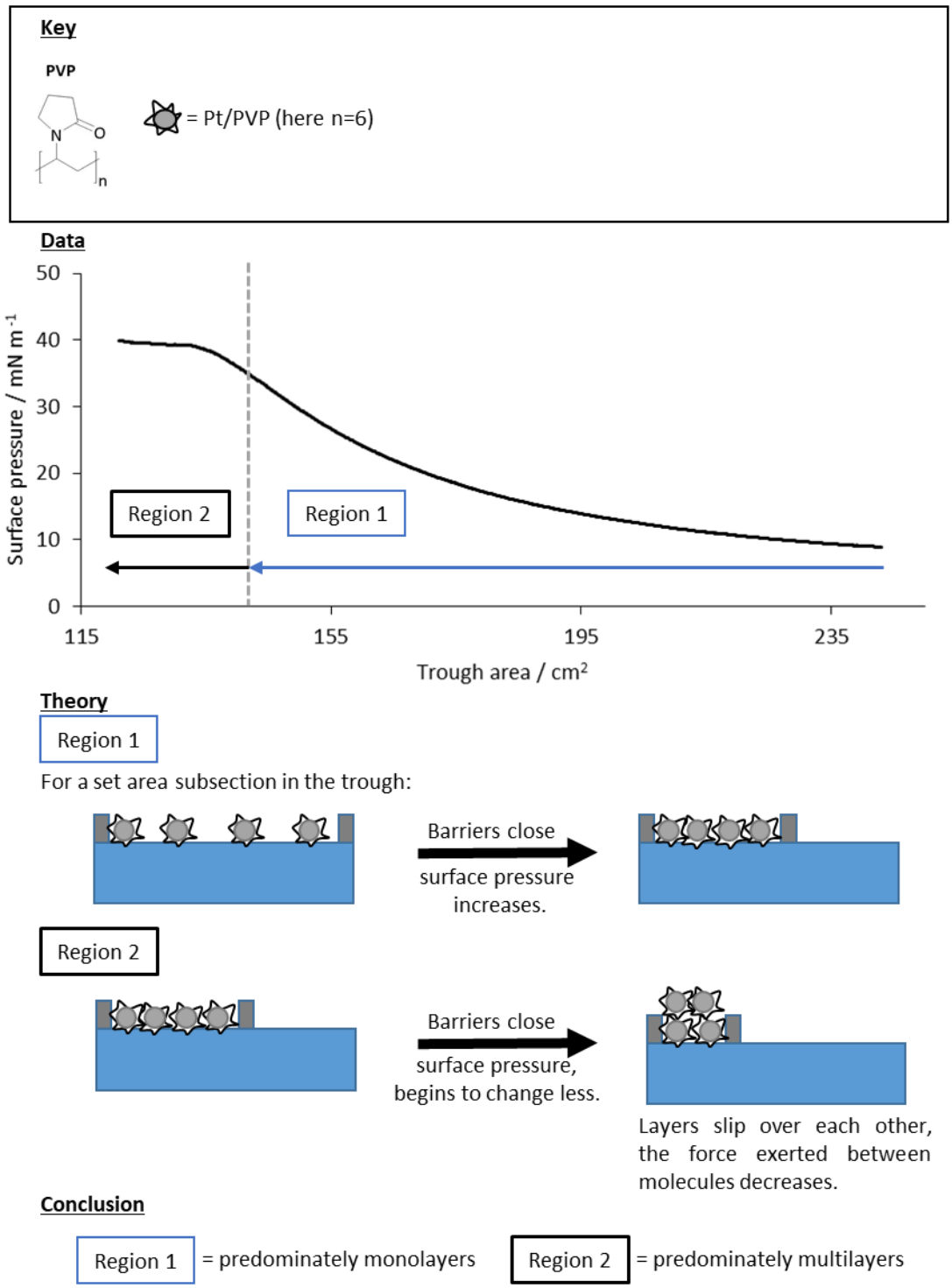

Figure 2.9. Diagram to depict changes in the interactions for a platinum/PVP nps (Pt/PVP), dispersed on the surface of the LB trough, upon closing of the troughs barriers (compressing the sample area).

2.1.7. Mesoporous support synthesis

The synthesis of the mesoporous silica supports such as SBA-15, and KIT-6 relies upon the self-assembly of the surfactant species.[29,30] This self-assembly takes place due to structure directing effect of the surfactant *via* interaction with the inorganic (silica) species. Early work by Firouzi *et al*. expanded upon the knowledge of such systems in order to allow for their controlled and more widespread use.[31] Techniques such as magnetic resonance spectroscopy, and small angle X-ray scattering were used to investigate the mesopores organisation of such materials. The authors found that self-assembly took place upon the addition of an aqueous basic solution, and anionic silicate oligomers.[31] It can be noted that Zhao *et al.* and Ryoo *et al.,*[29,30] used an acidic solution of hydrochloric acid in order to control the shape of the pores produced. Zhao *et al.* synthesised hexagonal mesoporous SBA-15 using hydrochloric acid,[29] and Ryoo *et al.* used butanol and hydrochloric acid to synthesise KIT-6 with a cubic morphology.[30] For the anionic silicate oligomer tetraethyl orthosilicate was used by Zhao *et al.,*[29] and tetraethoxysilane was used by *Ryoo et al*..[30] The chemistry is complex due to the aqueous silicate chemistry influencing the self-assembly,[31] but generally the behaviour can be compared to that of the more widely understood lyotropic liquid crystalline systems.[32] Zhao *et al.,*[29] further improved upon the traditional synthesis of SBA-15 by groups such as Firouzi *et al*.,[31] by using amphiphilic polymers (*e.g.* Pluronic 123) with high molecular weights as structure-directing agents in order to increase and allow for tunability of the pore size within the support. The same polymeric surfactant species was also used for the synthesis of KIT-6 with the same motivation.[30]

In the work of Somorjai *et al*.,[33] mesoporous cerium (IV) oxide was synthesised using KIT-6 mesoporous silica as a hard template – so-called nanocasting.[34,35] In nanocasting the desired structure is synthesised using a suitable template (with dimensions in the nanometer scale). The template is filled with the material of interest (in this case the cerium precursor), the precursor is decomposed to the oxide and subsequent removal of the template species results in formation of the desired final structure.[34] Either hard (such as carbon nanotubes, and mesoporous materials) or soft templates (such as surfactants, or chelating agents) can be used. In this case a hard templating agent was chosen. The use of hard templating in nanocasting has allowed for the synthesis of materials with high porosity,[36] and was selected in this case due to a variety of reported topological advantages including stability, predictability, and control.[34] KIT-6 was chosen as the template due to its mesoporous structure. This 3D pore structure was then in turn imparted upon the cerium(IV) oxide

support synthesised, as was confirmed by wide angle PXRD and nitrogen adsorption and desorption techniques.[35]

2.1.8. Plasma cleaning

Plasma cleaning has been used within this thesis for the removal of organic capping agents from deposited nanoparticle samples (Chapter 2, Sections 2.2.4.6, and 2.2.5.9) for application in TIR Raman spectroscopy. Plasma, an ionized gas consisting of positive ions, radicals and free electrons, interacts with the surface species upon the supported nanoparticle system resulting in the breaking up of the capping agent into smaller fragments. The surface species are therefore transformed into small gaseous, volatile products such as carbon dioxide, carbon monoxide and hydrogen.[37] These species are then removed using the vacuum of the plasma cleaning unit.

2.2 Experimental

2.2.1. Nanoparticles/catalytic materials

All solvents were bought from Fisher unless otherwise stated. All oleylamine used was supplied by Acros Organics with an approximate 80-90% C_{18} content. For any reactions conducted under an inert atmosphere the system was put under vacuum (typically 10^{-2} mbar) and then backfilled with inert gas (argon or nitrogen) and the process repeated three times. This represents statistically an atmosphere which contains essentially only the inert gas (99.999% of molecules are removed in each cycle). The inert gas is dried by passing through a moisture trap consisting of indicating phosphorus pentoxide and calcium chloride drying agents. All glassware was washed in a base bath (1 M potassium hydroxide in 2-propanol and water) and then rinsed with water, washed in an acid bath (1 M nitric acid) and again thoroughly rinsed with water before being air dried and then dried in a 100 °C oven overnight before use.

2.2.1.1. Platinum/PVP nps

2.2.1.1.1. Preparation

The preparation was taken from the work of Krier *et al.*.[38] The authors reported typical average particle sizes of 4.2 nm, and did not indicate typical yields. The reaction was clean (there were no precipitated products), and there was an excess of reducing agent, therefore it is assumed that the reduction reaction goes to completion.

In a typical preparation chloroplatinic acid hexahydrate (100 mg, 19 mmol) was added to polyvinylpyrrolidone (from Sigma Aldrich, 440 mg, 4.0 mmol, average M_w ~55,000) in a 2

neck round bottom flask. The flask was put under an argon atmosphere and ethylene glycol (20 mL) was added. The solution was stirred at 30 °C until all material had gone into solution. The contents of the flask were heated for 25 min at 165 °C. Dark brown/ black coloration was seen indicating nanoparticle formation. Once cooled to room temperature, reagent grade acetone (an antisolvent that affects precipitation of the nanoparticles) was added in a 3:1 volume ratio with respect to the product solution. The resulting solution was centrifuged (in a Thermo Scientific, Sorvall, Legend X1, centrifuge) at 6000 RPM for 10 min, or until complete precipitation occurred. The liquid phase comprising solvent, antisolvent and soluble impurities was decanted, and the solid residue was re-dispersed in the minimum possible volume of HPLC grade ethanol. A 5:1 volume ratio of reagent grade hexane relative to ethanol was then added to the solution to precipitate the nanoparticles, followed by centrifuging at 6000 RPM for 10 min, or until complete precipitation occurred. Again the liquid phase was decanted, and the product was dissolved in the minimum volume of HPLC ethanol. The process was repeated to give a total of 8 washes.

A particle size of 4 ± 1 nm was recorded from measurement of a minimum of 100 particles from TEM imaging (as detailed in Section 2.2.5.10).

2.2.1.1.2. Further Characterisation

Nuclear magnetic resonance (NMR) spectroscopy was recorded for the polyvinylpyrrolidone capping agent to allow characterisation of the polymers composition (Section 2.2.5.1), as well as identifying the presence of any impurities. Gel permeation chromatography (GPC) (recorded on a Viscotek TDA 302 complete with a GPC max autosampler, with tetrahydrofuran mobile phase with refractive index (RI) and right angle light scattering (RALS) detection) and UV-vis spectroscopy (Section 2.2.5.6) were conducted in order to confirm the purity of polyvinylpyrrolidone capping agent and the platinum nanoparticles with polyvinylpyrrolidone respectively.

2.2.1.2. *Platinum/oleylamine nanoparticles (platinum/OAm nps)*

Oleylamine capped platinum nanoparticles (platinum/OAm nps) were synthesised from adaptation of Mazumder *et al.,*[39] with the literature preparation using an initial temperature of 60 °C which was in our case increased to 100 °C, and the literature using a ripening temperature of 90 °C which was increased in our preparation to 120 °C. The temperature increase was used to facilitate the synthesis of nanoparticles with a smaller average size. The authors reported a particle size of 4.5 nm as determined from TEM images.

Platinum(II) acetylacetonate (purchased from Alfa Aesar, 50 mg, 0.1 mmol, 99.9% metal basis) was placed under nitrogen, and oleylamine (15 mL, 46 mmol as received from Acros Organics with no further purification conducted) was added. The mixture was stirred and heated to 100 °C in 20 min, with the temperature and heating rate controlled by a submerged K-type thermocouple and an omega CN 7500 PID controller. Borane trimethylamine (from Alfa Aesar 96% purity, 0.28 mL, 1.9 mmol) was injected quickly into the solution and the solution went from yellow to black, indicating colloidal particle formation. The solution temperature was ramped to 120 °C over 10 min, and this temperature was then held for 60 min. The reaction was stopped by submerging the reaction vessel in an ice bath. Once cooled to room temperature, HPLC grade ethanol (an antisolvent that effects precipitation of the nanoparticles) was added in a 3:1 volume ratio with respect to the product solution. The resulting solution was centrifuged at 6000 RPM for 10 min, or until complete precipitation occurred. The liquid phase comprising of solvent, antisolvent and soluble impurities was decanted and the solid residue was re-dispersed in the minimum possible volume of reagent grade hexane. A 5:1 volume ratio of HPLC grade ethanol relative to hexane was then added to the solution to precipitate the nanoparticles, followed by centrifuging at 6000 RPM for 10 min, or until complete precipitation occurred. Again the liquid phase was decanted, and the product was dissolved in the minimum volume of ethanol. The process was repeated 2 times. A further note on particle re-dispersion and precipitation is that a sonication bath (Bandelin Sonorex) was used to aid re-dispersion of the nanoparticle in hexane. If precipitation did not take place fully after centrifuging the nanoparticle solution the solvent volume was reduced and the antisolvent volume increased, the sample was then chilled in the freezer for several hours.

2.2.1.3. Cobalt/oleic acid nanoparticles (cobalt/OAc nps)

Cobalt/oleic acid nanoparticles (cobalt/OAc nps) were synthesised according to the procedure given by Iablokov *et al*..[40] Synthesis took place using an isomantle with the temperature and heating rate controlled by a submerged K-type thermocouple and an omega CN 7500 PID controller. Cobalt carbonyl was handled in a glove box prior to dissolving in o-dichlorobenzene under argon in a septum capped vial. Oleic acid (Acros Organics, 130 mg, 97% pure) in a 250 mL round bottom flask was placed under nitrogen and anhydrous o-dichlorobenzene (99%, DCB, 15 mL) was added. High purity oleic acid was used as Iablokov *et al*. had found that technical grade oleic acid produced unrepeatable results.[40] The flask was equipped with a long Liebig condenser and gas release line in order to accommodate the large volume of gas (carbon monoxide) produced upon rapid decomposition of the

carbonyl precursor. The solution was heated under stirring to the required temperature (168 °C). Once at temperature cobalt carbonyl (Alfa Aesar, 95%, stabilized with 1-5% hexane) in dichlorobenzene (3 mL, 0.5 M) was injected as quickly as possible into this solution (25 mL plastic syringe equipped with a large ID needle). The solution (initially brown) turned black immediately indicating nanoparticle formation. The solution was ripened for 20 min. The solution was then cooled to room temperature under a flow of air. In order to allow for precipitation dichlorobenzene (10 mL) and 2-proponal (ACS Grade, *ca.* 20 mL) were added to this suspension. The nanoparticles were then seperated by centrifugation (6000 RPM) and then decanted. The nanoparticle was re-dispersed and stored in 2-proponal.

A particle size of 9 ± 1 nm were recorded from measurement of a minimum of 100 particles from TEM imaging (as detailed in Section 2.2.5.10).

2.2.1.3.1. Oleylamine mass spectrometry and vacuum distillation

Oleylamine (60 mL) was charged into a flask equipped with a distillation head-condensor and collection flask, such that the entire setup could be placed under nitrogen. Once under nitrogen, vacuum was applied (1 Torr) and then the system was heated, with fractions removed at 80 °C, and 120 °C. The distilled solution was collected and the distillation stopped when around 10-15% by volume of the original starting solution remained.

2.2.1.4. Silver/oleylamine/oleic acid nanoparticles (silver/OAm/OAc nps) synthesised from Ag perchlorate

Silver/ oleylamine/oleic acid nanoparticles (silver/OAm/OAc) nps were synthesised based on adaptation of a procedure outlined by Koski *et al.*.[6] The authors did not report the product yield, and stated the silver nanoparticle diameter ranged from 5-10 nm as a function of ripening time 2 min to 24 h. The term *ripening time* denotes the period for which the sample was held at an elevated temperature, in which particle size or shape changes might be expected to take place. Preparations took place in amber stained glassware (round bottom flask, condenser, stoppers) due to the light sensitive nature of silver perchlorate.

In a typical preparation 1,2-tetradecanediol (from Sigma Aldrich, 129 mg, 0.5 mmol, technical grade 90%) was added to oleylamine (177 mg, 0.6 mmol) in a two neck flask fitted with a condenser. The vessel was placed under an inert atmosphere, and the contents of the flask was then refluxed in anhydrous toluene (12.92 mL). Once at reflux, a solution of silver perchlorate from (Alfa Aesar 48 mg, 0.25 mmol, 99.95% metal basis) in anhydrous toluene (0.2 mL) stored/prepared in a foil wrapped vial, was added to the vessel. The solution was

held at reflux for the specified ripening time (either 2 min or 1 h), oleic acid (from Acros Organics, 0.1 mL, 97% pure) was then added. Once cooled to room temperature, reagent grade 2-propanol (an antisolvent that affects precipitation of the nanoparticles) was added in a 3:1 volume ratio with respect to the product solution. The resulting solution was centrifuged at 6000 RPM for 10 min, or until complete precipitation occurred. The liquid phase comprising solvent, antisolvent and soluble impurities was decanted, and the solid residue was re-dispersed in reagent grade 2-propanol with sonication. The solution was centrifuged at 6000 RPM for 10 min, or until complete precipitation. Again the liquid phase was decanted, and the washing process repeated to give a total of 8 washes. The product was dissolved in the minimum volume of HPLC grade hexane. A further note on particle re-dispersion and precipitation is that a sonication bath (Bandelin Sonorex) was used to aid re-dispersion of the nanoparticle in hexane. If precipitation did not take place fully after centrifuging the nanoparticle solution the solvent volume was reduced and the antisolvent volume increased, the sample was then chilled in the freezer for several hours.

The antisolvent and solvent used in the washing procedure was established using three differing initial systems; 2-propanol and hexane, 2-propanol and pentane, and just 2-propanol to re-disperse the material rather than first dissolve it. From these systems the latter was found optimal as the nanoparticles would not readily precipitate from the hydrocarbon solvents.

Particle sizes of 6 ± 1 nm were recorded by TEM for both ripening times.

2.2.1.5. Copper nanoparticles

The preparation has been extensively adapted, though initially took inspiration from Mott *et al.* and Koski *et al.*.[41,6] Initially the amounts of oleylamine and oleic acid used were altered based on the required amount estimated to equal full coverage of the surface of the nanoparticle, based on the following crude calculation.

2.2.1.5.1. Calculation of the amount of oleylamine capping agent required to give full coverage of copper surface

For a small copper nanoparticle with a diameter of 3 nm, the total surface area available for the capping agent to bind to is 2.8×10^{-17} m^2 per particle. For capping agent binding in the head-on orientation (Figure 2.10) an estimation of the maximum number of capping agents bound can be made. The number of capping agents bound to one 3 nm diameter copper nanoparticle, can be determined from the van der Waals dimensions of the head group. Since

such data was not readily available for oleylamine calculations made use of values for the thiol group instead. This was on the basis that the thiol was likely an upper limit (would be larger than the amine). For a typical thiol head group the van der Waals dimensions were 5.29×10^{-20} m^2.[42]

This gives an approximation of 530 capping agents which could bind head on around one 3 nm copper nanoparticle.

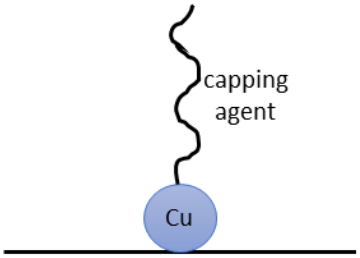

Figure 2.10. Schematic of copper (Cu) nanoparticle with capping agent bound in a head on fashion.

The number of copper atoms in the particle of diameter 3 nm can be estimated. The fcc unit cell for copper is shown below in Figure 2.11.

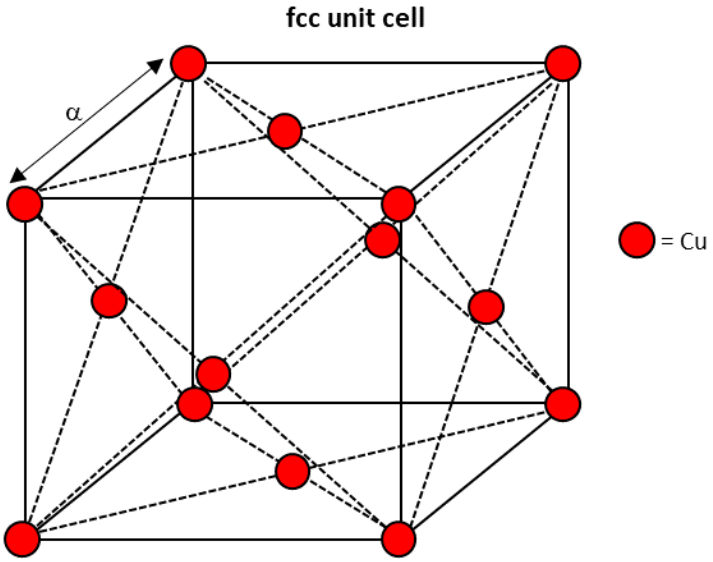

Figure 2.11. Diagram of fcc unit cell for copper (Cu).

The lattice vector α can be calculated from the atomic radius (R) for copper using Equation 2.7.

$$a = 2\sqrt{2}R \qquad \textit{Equation 2.7}$$

Inputting of the value of R for copper allows for calculation of α.

$$a = 2\sqrt{2}(1.28 \times 10^{-10}\, m)$$

The volume occupied by an fcc unit cell (V) can be given by Equation 2.8.

$$V = a^3 \qquad \textit{Equation 2.8}$$

$$V = ((2\sqrt{2})(1.28 \times 10^{-10}\, m))^3$$

$$V = 4.7 \times 10^{-29}\, m^3$$

The volume (V_S) occupied by the copper nanoparticle of diameter 3 nm can then be calculated, as shown in Equation 2.9.

$$V_s = \frac{4}{3}\pi r^3 \qquad \textit{Equation 2.9}$$

$$\mathrm{V_s} = \frac{4}{3}\pi(1.5 \times 10^{-9}\, m)^3$$

$$\mathrm{V_s} = 1.4 \times 10^{-26}\, m^3$$

Therefore the number of copper fcc unit cells (N) which can fit in the 3 nm nanoparticle is given by Equation 2.10.

$$N = \frac{V_S}{V} \qquad \textit{Equation 2.10}$$

$$\mathrm{N} = \frac{1.4 \times 10^{-26}\, m^3}{4.7 \times 10^{-29}\, m^3}$$

$$N = 300$$

Given that 4 copper atoms occupy one unit cell this gives a value of approximately 1200 copper atoms per 3 nm nanoparticle.

The molar ratio of capping agent:copper required to only fully saturate the surface of the copper nanoparticle, based on the assumptions above for a 3 nm particle, is therefore around 1 : 2. In contrast to the larger excess used in the prior work of Mott *et al.* and Koski *et al.* (which can be subsequently difficult to remove),[41,6] a starting point and the standard preparation that follows reduced the ratio to one order of magnitude more capping agent than was believed to be needed – a capping agent:copper precursor molar ratio of 5:1 (equating to a capping agent: copper molar ratio of 20:1). This was chosen to still assert a significant excess was present.

2.2.1.5.2. Standardised preparation

Initial experimentation used an oil bath, but greater control of reaction temperature was achieved using an isomantle with the temperature and heating rate controlled by a submerged K-type thermocouple and an omega CN 7500 PID controller. All preparations of copper nanoparticles detailed within this report were prepared using an isomantle, PID controller and thermocouple in this configuration. For all preparations the solvent diphenyl ether was dried over molecular sieves and degassed prior to use. In a typical preparation oleylamine (80-90% approximate C_{18} content, from Acros Organics, 0.36 mL, 1.1 mmol, used as purchased with no further purification or drying), in a two neck flask fitted with a condenser, was placed under inert atmosphere, and diphenyl ether (10.00 mL) was added and stirred and the mixture was heated to 200 °C. Once at 200 °C copper(II) acetylacetonate (from Sigma Aldrich, 60 mg, 0.23 mmol, 99.99% trace metal basis) was prepared in pyridine (0.4 mL), the solution was added to the hot reaction mixture, to give fast reduction and a controlled start to the particle nucleation and growth process. Upon addition the solution goes black. Colouration then typically goes through brown, to purple, indicating nanoparticle growth. After a 1 h ripening time the product was cooled to room temperature using an ice bath. The resulting nanoparticles were then washed in a 2-propanol antisolvent and hexane solvent system. A further note on particle re-dispersion and precipitation is that a sonication bath was used to aid re-dispersion of the nanoparticle in hexane. If precipitation did not take place fully after centrifuging the nanoparticle solution the solvent volume was reduced and the antisolvent volume increased, the sample was then chilled in the freezer for several hours.

Within this standardised preparation a variety of variables were explored as are summarised in Table 2.1. Two parameters for which the experimental procedure was varied from that given above are that of reducing agent addition, and metal complexation as described in the sections below.

Table 2.1. A summary of key parameters varied within the standard preparation.

Parameter	Variables tried
Solvent	Diphenyl ether.
Capping agent	Oleylamine, oleylamine and oleic acid and octadecylamine.
Ripening temperature	200 to 240 °C.
Ripening time	10, 30, 60, 120, 180, 240 min.
Reducing agent	None unless stated.
Procedure	Metal precursor injected at temperature.

2.2.1.5.2.1. Reducing agent

If reducing agent was used, morpholine borane complex (from Alfa Aesar, 0.023 g, 0.23 mmol, 97% purity) or 1,2-tetradecanediol (from Sigma Aldrich, 0.053 g, 0.23 mmol, technical grade 90%) was added to diphenyl ether (3 mL) and stirred for several hours at 80 °C in a two neck flask fitted with a condenser, which had been placed under inert atmosphere, until fully in solution. The solution was then injected into a solution of oleylamine (0.36 mL, 1.1 mmol) and diphenylether, dried over molecular sieves and degassed (7 mL) solution. The sample was then heated to 200 °C and continued as specified above (Section 2.2.1.5.2).

2.2.1.5.2.2. Oleylamine and metal complexation

Complexation of metal and capping agent was achieved by stirring a solution of oleylamine (0.36 mL, 1.1 mmol) and copper(II) acetylacetonate (from Sigma Aldrich, 60 mg, 0.23 mmol, 99.99% trace metal basis) in diphenylether overnight at 80 °C, (3 mL/10 mL depending upon whether reducing agent was/was not required). If reducing agent was not required the solution was then heated to 200 °C, ripened for 1 h and washed as usual.

If reducing agent was required, the solution was heated to 175 °C (*i.e.* a temperature below which reduction will occur in absence of a reducing agent), and morpholine borane complex (Alfa Aesar, 0.046 g, 0.46 mmol, 97% purity) in diphenyl ether (7 mL) (stirred for several hours until fully in solution) was quickly added. The solution was then ripened for 1 h at 180 °C.

After a 1 h ripening time the product was cooled to room temperature using an ice bath, and washed as specified above (Section 2.2.1.5.2).

2.2.1.5.2.3. Full list all preparation conditions trialled

A full list of all experimental conditions tried for copper nanoparticle synthesis, along with the corresponding Figure numbers (Chapter 4) and the file location for full TEM data (Electronic Supplementary Information) are given in Chapter 4 Appendix Table 4A.1.

2.2.1.5.3. Silver nanoparticles from silver(I) acetylacetonate

Experimentation took place using an isomantle with the temperature and heating rate controlled by a submerged K-type thermocouple and an omega CN 7500 PID controller. For all preparations the solvent diphenyl ether was dried over molecular sieves and degassed prior to use. Silver(I) acetylacetonate (from Sigma Aldrich 98% pure), was weighed in a glove box under light sensitive conditions and stored in a foil wrapped Schlenk tube prior to use. Preparations took place in amber stained glassware (round bottom flask, condenser, stoppers) due to the light sensitive nature of silver(I) acetylacetonate. In a typical preparation morpholine borane complex (from Alfa Aesar, 0.046 g, 0.46 mmol, 97% purity) was added to diphenyl ether (10.00 mL) and stirred at 80 °C for several hours until fully in solution. To this solution octadecylamine (0.29 g, 1.1 mmol) was added, and the mixture was heated to 200 °C under stirring. Once at 200 °C silver(I) acetylacetonate (48 mg, 0.23 mmol) was prepared in pyridine (0.4 mL), the solution was added to the hot reaction mixture, to give fast reduction and a controlled start to the particle nucleation and growth process. After a 1 h ripening time the product was cooled to room temperature using an ice bath. The resulting nanoparticles were then washed in 2-propanol antisolvent and hexane solvent systems. The resulting nanoparticle system is typically black in colour.

TEM characterisation gave an average particle diameter 2 ± 1 nm.

2.2.1.6. Bimetallic silver and copper nanoparticles

Experimentation took place using an isomantle with the temperature and heating rate controlled by a submerged K-type thermocouple and an omega CN 7500 PID controller. For all preparations the solvent diphenyl ether was dried over molecular sieves and degassed prior to use. Silver(I) acetylacetonate (from Sigma Aldrich 98% pure) was weighed in a glove box under light sensitive conditions and stored in a foil wrapped Schlenk tube prior to use. Preparations took place in amber stained glassware (round bottom flask, condenser, stoppers) due to the light sensitive nature of silver(I) acetylacetonate. In a typical preparation

morpholine borane complex (from Alfa Aesar, 0.023 g, 0.23 mmol, 97% purity) was added to diphenyl ether (10.00 mL) and stirred at 80 °C for several hours until fully in solution. To this solution octadecylamine (0.29 g, 1.1 mmol) was added, and the mixture was heated to 220 °C under stirring. Once at 220 °C two solutions of silver(I) acetylacetonate (24 mg, 0.12 mmol) prepared in pyridine (0.2 mL), and copper(II) acetylacetonate (from Sigma Aldrich, 30 mg, 0.12 mmol, 99.99% trace metal basis) in pyridine (0.2 mL), with both solutions added in quick succession to the hot reaction mixture, to give fast reduction and a controlled start to the particle nucleation and growth process. After a 1 h ripening time the product was cooled to room temperature using an ice bath. The resulting nanoparticles were then washed in 2-propanol antisolvent and hexane solvent systems.

A first attempt of this preparation was run using the procedure given above but using an increased concentration of morpholine borane complex from (Alfa Aesar 0.046 g, 0.46 mmol, 97% purity), and a reduced preparation temperature of 200 °C.

TEM characterisation gave an average particle diameter 5 ± 2 nm for the first preparation at 200 °C with an increased concentration of morpholine borane complex, and 7 ± 4 nm for the increased 220 °C preparation temperature and lowered concentration of morpholine borane complex.

2.2.1.6.1. List of preparation conditions used for bimetallic silver and copper nanoparticles

A full list of all experimental conditions tried for silver monometallic and silver and copper bimetallic nanoparticle synthesis, along with the corresponding Figure numbers (Chapter 4) and the file location for full TEM data (Electronic Supplementary Information) is given in Table 2.2.

Table 2.2. Full list of experimental conditions tried for silver monometallic and silver and copper bimetallic nanoparticles (Ag, and AgCu) synthesis (synthesised with a 0.115 : 0.115 mmol ratio of silver(I) acetylacetonate : copper(II) acetylacetonate), with octadecylamine (ODA) capping agent, and morpholine borane complex (mbc) reducing agent. The corresponding Figure numbers (Chapter 4) and the file locations for full TEM data (referring to locations within the Electronic Supplementary Information) are given where Section-Figure refers to the Section of Chapter 4 and the parameter being varied and, Figure is the Figure number and Spectra letter (A, B, C etc.) of interest (e.g. 4.24 is Figure 4.24). Within this terminology the following section abbreviations were used: Ag: silver monometallic section, AgCu: silver and copper bimetallic synthesis, precipitate (ppt.). An N/A entry, in the particle diameter and standard deviation columns, corresponds to no nanoparticles being received and so no TEM imaging undertaken. It should be noted that for all TEM data given in the sections that follow particle size for spherical or oval shapes were counted by their typical diameter. Hexagonal shapes were calculated using their long diameter (perhaps resulting in very slightly overestimating their size), but for cubes a mathematical average of their longest (corner to corner) and shortest (side to side) cross particle lengths was used.

Sample	Section-Figure	Temperature / °C	Ripening time / h	Capping agent	Moles capping agent / mmol	Reducing agent	Moles reducing agent / mmol	Colour of solution	Diameter from TEM / nm	Standard deviation / nm	Tem location
Ag_290716_1	Ag-4.24	200	1	ODA	1.1	mbc	0.46	black	2	1	microscopy-2016-9/8/16
AgCu_010816_1	AgCu-4.25	200	1	ODA	1.1	mbc	0.46	pale brown, black ppt.	5	2	microscopy-2016-9/8/16 10/8/16
AgCu_080816_1	AgCu	200	1	ODA	1.1	mbc	0.92	clear, purple ppt.	N/A	N/A	N/A
AgCu_150816_1	AgCu-4.26	220	1	ODA	1.1	mbc	0.23	brown/black	7	4	microscopy-2016-17/8/16

2.2.1.7. Copper nanoparticles doped with platinum to give a material with the following molecular structure of platinum$_{0.18}$copper$_{15}$/alumina

First copper nanoparticles were synthesised using optimised preparation conditions (Section 2.2.1.5), which are known to result in the formation of small monodisperse particles with a particle size distribution of 6 ± 1 nm. The preparation details are given below.

In a typical preparation morpholine borane complex (from Alfa Aesar, 0.024 g, 0.46 mmol, 97% purity) was added to diphenyl ether (10 mL), dried over molecular sieves and degassed, and stirred for several hours at 80 °C until fully in solution. Octadecylamine (0.29 g, 1.1 mmol) was injected into the solution. The solution was then heated to 200 °C and stirred. Once at temperature a solution of copper(II) acetylacetonate (from Sigma Aldrich, 60 mg, 0.23 mmol, 99.99% trace metal basis) in pyridine (0.4 mL) was added to the hot reaction mixture, to give fast reduction and a controlled start to the particle nucleation and growth process. Upon addition the solution goes black. The solution was ripened for 1 h. Colouration then typically goes through brown, to purple, indicating nanoparticle growth. A solution of platinum(II) acetylacetonate (5 mg, 1.3 µmol) in diphenyl ether (10 mL) was prepared, from which 1 mL was extracted and added to the 1 h ripened copper solution. The solution was stirred under nitrogen for 10 min, upon which no change in colour was seen. The product was then cooled to room temperature using an ice bath. The resulting solution was centrifuged at 6000 RPM for 10 min, or until complete precipitation occurred. The liquid phase comprising solvent, antisolvent and soluble impurities was decanted, and the solid residue was re-dispersed in the minimum possible volume of HPLC grade hexane. A 5:1 volume ratio of reagent grade 2-propanol relative to hexane was then added to the solution to precipitate the nanoparticles, followed by centrifuging at 6000 RPM for 10 min, or until complete precipitation occurred. Again the liquid phase was decanted, and the product was dissolved in the minimum volume of HPLC hexane. The process was repeated to give a total of 1 wash. A further note on particle re-dispersion and precipitation is that a sonication bath (Bandelin Sonorex) was used to aid re-dispersion of the nanoparticle in hexane. If precipitation did not take place fully after centrifuging the nanoparticle solution the solvent volume was reduced and the antisolvent volume increased, the sample was then chilled in the freezer for several hours.

2.2.1.8. Palladium/oleylamine nanoparticles (palladium/OAm nps)

Palladium nanoparticles were synthesised from adaptation of the preparation from Mazumder and Sun,[39] modified to use a more readily available amine-borane complex. In a typical preparation palladium(II) acetylacetonate (73 mg, 0.2 mmol) was placed under an

inert atmosphere, and oleylamine (15 mL, 46 mmol, Acros Organics, 80-90%) was added. The mixture was stirred and heated to 60 °C. Borane trimethylamine (from Alfa Aesar, 96% purity, 0.52 mL, 3.5 mmol) was added to the solution and the solution went from pale yellow to pale brown. The solution temperature was ramped to 90 °C, over 15 min giving rise to a black solution indicating nanoparticle formation, and this temperature was then held for 60 min. Once cooled to room temperature, HPLC grade ethanol (an antisolvent that effects precipitation of the nanoparticles) was added in a 3:1 volume ratio with respect to the product solution. The resulting solution was centrifuged at 6000 RPM for 10 min, or until complete precipitation occurred. The liquid phase comprising solvent, antisolvent and soluble impurities was decanted, and the solid residue was re-dispersed in the minimum possible volume of reagent grade hexane. A 5:1 volume ratio of HPLC grade ethanol, relative to hexane, was then added to the solution to precipitate the nanoparticles, followed by centrifuging at 6000 RPM for 10 min, or until complete precipitation occurred. Again the liquid phase was decanted, and the product was dissolved in the minimum volume of ethanol. The process was repeated 8 times. A further note on particle re-dispersion and precipitation is that a sonication bath (Bandelin Sonorex) was used to aid re-dispersion of the nanoparticle in hexane. If precipitation did not take place fully after centrifuging the nanoparticle solution the solvent volume was reduced and the antisolvent volume increased, the sample was then chilled in the freezer for several hours. TEM characterisation gave an average particle diameter 6 ± 1 nm. Extending the length of particle aging at 90 °C to 90 min (with the same initial ramp rate) allowed for the synthesis of larger nanoparticles of 5.6 $\pm$ 0.8 nm diameter for use in hierarchical structured materials (Chapter 6, Section 6.3). Inductively coupled plasma-optical emission spectrometry (ICP-OES) analysis of the palladium content of this second nanoparticle solution gave a value of 11.0 $\pm$ 0.12 mg (in 30 mL), indicating around 43% of the initial palladium was present in the nanoparticles after purification.

2.2.2. Attempted purification of fluorescent species from polyvinylpyrrolidone

2.2.2.1. Purification-Soxhlet extraction

As described in Chapter 3, an attempt was made to further purify polyvinylpyrrolidone using Soxhlet extraction. A typical Soxhlet set-up was used is shown in Figure 2.12. Ultra-High Purity (UHP) water used as the extraction solvent for the polyvinylpyrrolidone nanoparticles. The flask was thoroughly lagged and heated to the boiling point of extraction solvent (around 100 °C). The equipment was then adjusted so that the solvent dripped from the condenser to the extraction thimble. The solvent was then collected in the extraction chamber, and when the chamber was full it was emptied into the flask below. Several iterations of solvent

collection and emptying took place. The product was dried by rotary evaporation and made to a 1mg mL^{-1} solution in ethanol for study *via* UV-vis spectroscopy. Extraction also took place using a dialysis bag, due to the solubility of polyvinylpyrrolidone in water it was suspected that material might pass through the thimble into the main solution and so not undergo the extraction process.

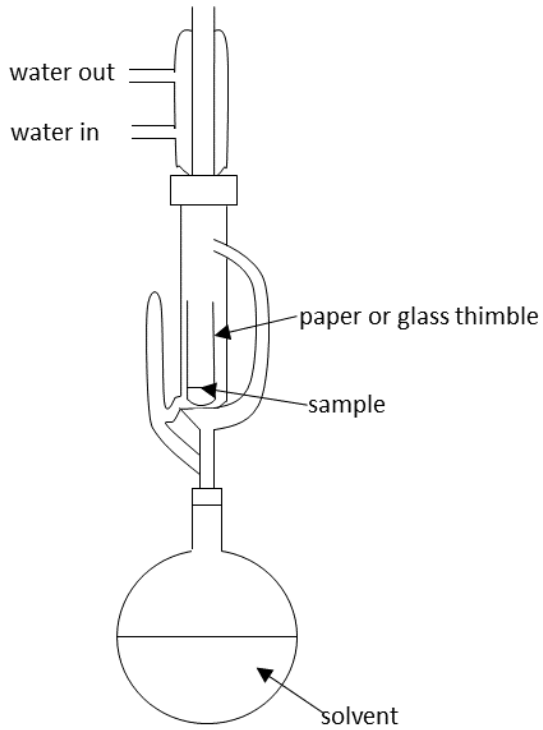

Figure 2.12. Diagram to show experimental set-up (under air) for Soxhlet extraction.

2.2.3. Catalyst supports

2.2.3.1. SBA-15 mesoporous silica

SBA-15 was prepared as reported by Pushkarev *et al.,*[43] who also reported the as prepared material had a Brunauer–Emmett–Teller (BET) surface area of 950 $m^2 g^{-1}$, a pore volume of 2.5 $m^2 g^{-1}$ and a pore diameter of 9 nm as determined by nitrogen porosimetry.

The preparation was conducted in a sealed 500 mL polypropylene bottle, with a well-fitting lid, by adding Pluronic P-123 (M_w ~5,800 (specified by manufacturer); 8 g, 1.4 mmol), to distilled water (60 mL) and hydrochloric acid (2 M, 240 mL). The resulting mixture was stirred and heated to 45 °C, on a water bath, for 30 min. Tetraethyl Orthosilicate (TEOS) (17 g, 82 mmol) was then added, and the mixture was stirred at 45 °C for 20 h. The solution was then aged at 100 °C for 24 h in a standard convection oven (within the sealed polypropylene bottle) without stirring. The resulting viscous material was carefully filtered, and washed in

ethanol and water. The product was then calcined at 550 °C for 4 h in a furnace, in order to remove the template.

SBA-15 was characterised using TEM and Barrett-Joyner-Halenda (BJH) analysis by a masters student Harriet Barker (HB) and were not repeated in this work. From TEM various pore and channel measurements were made a summary of which is given in Table 2.3. The BJH pore size diameter was 7.0 ± 1 nm.

Table 2.3. Comparison of literature values and those measured in-house, for pore and channel properties of SBA-15 measured from TEM imaging, for material synthesised according to Pushkarev et al..[43]

	Distance between channels /nm	**Pore size diameter / nm**	**Pore width diameter / nm**
Literature[43]	7 -12	5-10	≈2
Measured	10-12	6-8	2-5

2.2.3.1.1. The synthesis of hierarchically ordered mesoporous-macroporous SBA-15

As part of collaboration with Aston and Leeds University hierarchically bimodal SBA-15 was synthesised.[44] The following porous support was synthesised by Christopher M. A. Parlett as described. In order to allow for the incorporation of polystyrene nanospheres (as a macropore directing template) a true liquid crystal templating technique was used.[45] Pluronic P123 (2 g) was sonicated with hydrochloric acid-acidified water (pH 2, 2 g) at 40 °C to a homogeneous gel. Tetramethoxysilane (4.08 cm^3) was added and stirred rapidly for 5 min at 800 RPM to form a homogeneous liquid, immediately followed by addition of the polystyrene colloidal crystals (6 g ground to a fine powder) added with agitation at 100 RPM for 1 min in order to homogenize the mix. The resulting viscous mixture was heated under vacuum (100 mbar) at 40 °C to remove the evolved methanol. After 2 h the solid was exposed to the atmosphere at room temperature for 24 h to complete precursor condensation.

Hierarchically ordered silica (10 g) (Section 2.2.3.1) was stirred into toluene (100 mL) for 1 min at -8 °C. Vacuum filtration was then used for retrieval of the solid which was then washed in cold toluene. The process was repeated four times to give full extraction of the polystyrene template. The solid received (2 g) was stirred into triethoxy(octyl)silane (6 mL) for 3 min and recovered by vacuum filtration before drying overnight at room temperature. This step introduced hydrophobic character selectivity into the macropores. The macroporous solid

(~2 g) was then refluxed in methanol (400 cm^3) for 18 h in order to give full extraction of the mesopore-directing agent (Pluronic P123) recovered by filtration. The material was washed three times with methanol in order to give a macroporous–mesoporous support with differing hydrophobicity between the interconnected pore networks.

2.2.3.2. Cerium (IV) oxide mesoporous ceria

Mesoporous ceria was synthesised following the work of Somorjai *et al*..[33] The preparation was chosen due to the low calcination temperature (300 °C), as a variety of literature procedures reported low surface areas, due to sintering of the support in the final calcination step.[46,47] A high surface area and large pore size was desired in order to allow deposition of nanoparticles into the support's pores. As part of the preparation KIT-6 mesoporous silica was used as a template allowing for the synthesis of ceria with a high surface area and pore size. Therefore it was necessary to first prepare KIT-6 as detailed below.

KIT-6 mesoporous silica preparation

KIT-6 mesoporous silica was synthesised according to Ryoo *et al.,*[48] in a 500 mL polypropylene bottle with a screw fit lid, by adding Pluronic P123 (M_w ~5,800 (specified by manufacturer); 8 g, 1.4 mmol) to distilled water (144 mL) and hydrochloric acid (35%, 6.7 mL, 13 mmol). The solution was stirred, on a water bath, at 35 °C until homogeneous. Butanol (4 g, 53 mmol) was then added and stirred, at 35 °C, for 1 h. Then TEOS (8.6 g, 42 mmol) was added, the temperature kept constant, and the mixture left to stir for 24 h.

The product was then aged, without stirring in the sealed polypropylene bottle, at 100 °C in a convection oven for 24 h. The viscous material was then filtered, whilst hot, and dried in air for 24 h. It was then washed in ethanol and hydrochloric acid, in order to remove the surfactant. The product was then calcined, in a furnace, at 550 °C for 6 h, in order to remove the template.

KIT-6 was then characterised by XRD and TEM. XRD showed peaks at 2θ 0.95, 1.09 and 1.79, which were be assigned to KIT-6 and the *Ia*3h*d* phase.[49]

Subsequent cerium (IV) oxide preparation

In a typical preparation cerium (III) nitrate hexahydrate (14 g, 32 mmol) was added to a 250 mL round bottomed flask with 16 mL of deionised water, with vigorous stirring until full dissolution took place. The temperature was raised from room temperature to 65 °C, and KIT-6 (8 g) and 100 mL toluene were added with stirring. The resulting solution was transferred to a large glass dish where the toluene was able to evaporate with continuous

stirring at 65 °C, and the remaining powder was dried and calcined at 300 °C for 6 h in air. In order to allow removal of the template a 2 M sodium hydroxide aqueous solution (200 mL) was heated to 60 °C and washed through the product powder using a Buchner funnel, and the final product was dried fully in an oven at 60 °C producing a pale yellow powder.

BET characterisation gave a surface area of 40.9 ± 0.2 $m^2 g^{-1}$ which was considerably smaller than the 150 $m^2 g^{-1}$ given in the work of Somorjai *et al*..[50]

2.2.3.3. Supporting nanoparticles/ catalytic materials

Nanoparticle catalysts employed in Chapter 6 were synthesised by supporting of the constituent nanoparticles (Section 2.2.1) or a metal precursor (silver nitrate in the case of Satsuma type catalysts,[51] as described in Section 6.1.1) upon support materials using a capillary inclusion procedure as described below. It should be noted that silica gel and alumina were purchased from Sigma Aldrich and subsequently treated in the manner described herein. All catalyst support materials were first finely ground with a pestle and mortar and passed through a 355 µm sieve. The support was then evacuated overnight in a Schlenk tube under vacuum at 100 °C (using a sand bath) in order to ensure no water remained in the support's pores. The material to be deposited (typically 1-10 wt.% metal) was then added to the support under a vigorous argon flow, with the solvent added dropwise until full immersion of the material had taken place. The solution was held under argon for at least 10 min, to stabilise before sonication under air for 1 h. Centrifugation was used (5000 RPM, 10 min or until precipitation occurred) in order to remove the solvent from the supported material. The solvent was decanted from the supported catalyst material. The material was dried overnight in the oven at 80 °C. If calcination was required around 250 mg of the supported catalyst was loaded into the centre of a ¼" OD quartz tube, resulting in a maximum length of 2 inches of powder to ensure a consistent temperature across the sample once in the furnace. The powder was held in place in the quartz tube with glass wool plugs on the downstream side. A wire was attached fixed at the exit of the tube and the wire pushed inside the downstream end of the tube to prevent the glass wool plug moving once gas was flowed through the tube.

2.2.3.3.1. Supporting of platinum and palladium nanoparticles upon bimodal ordered SBA-15

The platinum containing molecule was deposited selectively within the mesopores of the bimodal hierarchically ordered SBA-15 using incipient wetness impregnation in an aqueous solution of dihydrogen hexachloroplatinate (from Sigma Aldrich, ACS reagent grade). The support (0.6 g) was stirred in the aqueous salt solution (3 cm^3, 0.01575 g platinum salt,

nominal 1 wt.% loading) for 18 h in the dark. A dry powder was obtained by gentle heating of the slurry at 50 °C for 10 h. This was followed by reduction at 100 °C under hydrogen (flow rate 10 mL min^{-1}) for 1 h. The bimetallic palladium macropore/platinum mesopore material was further synthesised from this platinum supported material (0.3 g) using impregnation with a 6.5 mL solution of palladium nanoparticles (Section 2.2.1.8) in hexane (0.46 mg of palladium nanoparticle, nominal 1 wt.% loading). The resulting solid was stirred in solution for 1 h followed by solvent evaporation at room temperature resulting in the formation of a dry powder.

2.2.4. Raman and TIR Raman spectroscopy

During this work three independent Raman systems were used, System 1 was a modified Renishaw Raman Microscope, System 2 was an existing home built optical bench system and System 3 was purposefully constructed for using with catalyst *in situ* cells as part of this project.

2.2.4.1. System 1: 532 nm

System 1 (Figure 2.13) used a Laser Quantum Opus, frequency-doubled diode-pumped neodymium-doped yttrium orthovanadate laser at an excitation wavelength of 532 nm. The laser was a continuous wave (CW) laser with 2 W of power (Class 4) producing 8 mW of power at the sample when passed through two 10^1 optical density filters (the number of filters and laser power can be altered, any alteration made were noted). The beam delivery took place *via* mirrors on the laser table, the beam can either be delivered *via* the objective or *via* an external beam path at various angles (73° was used within this work). The beam was expanded to a diameter of 4-8 mm and then directed externally into the sample with a spot area of 4300 square micron using a focusing lens positioned between the mirrors and the sample. Once in the spectrometer (a Renishaw Ramascope) the Raman scattered light was directed into the detector. The beam block was positioned behind the sample.

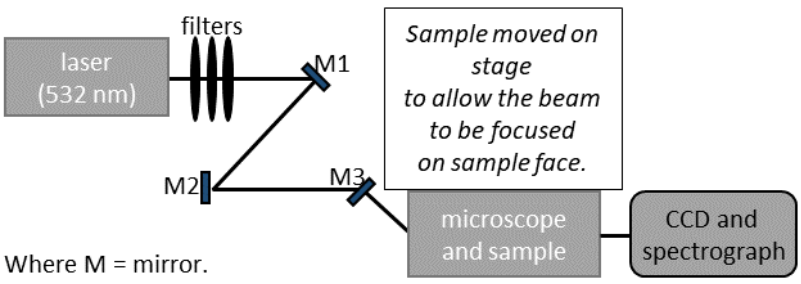

Figure 2.13. Schematic of set-up for System 1 (fitted with a 532 nm laser) used for confocal Raman spectroscopy.

The set-up was calibrated and the optics aligned before experimentation. Calibration took place initially using either a neon or mercury-argon lamp, then any offset was corrected with the 520 cm^{-1} shift of silicon. Alignments were carried out as follows: the mirrors were first positioned so that the laser passed through them centrally, fine manipulations were then carried out using a vertical ruler following a line on graph paper. During alignment the beam was focused onto the hemisphere centre using a microscope and CCD camera and by steering of the lenses in the x and y direction, and then aligned to give the required angle of incidence. The collection optics were aligned using the same silicon peak. The incident angle of the beam could be varied at this point. With a larger incident angle allowing for a larger sample spot, which was advantageous to attempting to reduce laser induced damage.

2.2.4.1.1 Bulk Raman spectroscopy

Bulk Raman spectroscopy took place using System 1 (as described above Section 2.2.4.1). Samples were prepared by drop casting onto a suitable support (typically a glass or silicon wafer) using the method described in Section 2.2.4.4.2.

Bulk Raman spectroscopy also took place using System 3 (Section 2.2.4.3). The lower 200 mW laser power setting was used for obtaining bulk spectra (where the higher sample concentration did not require such high laser powers).Two classes of samples were prepared. Bulk samples of selected capping agents were prepared by deposition within a glass capillary tube. Drop cast samples were also prepared using the methodology described below (Section 2.2.4.4.2).

2.2.4.2. System 2: 532 nm / 660 nm

The system (Figure 2.14) was fitted with two lasers: a 660 nm 1W Laser Quantum Ignis, and a 532 nm Spectra-Physics Millennia II, 2 W Frequency doubled neodymium-doped yttrium orthovanadate ($NdYVO_4$) laser. The 660 nm laser was chosen for experimentation in order to reduce fluorescent background signal. An incident angle of 73° was set. Calibration took place initially using either a neon or mercury-argon lamp, then any offset was corrected with the 520 cm^{-1} shift of silicon. Alignment (of the incident beam) was carried out using a vertical ruler following a line on graph paper. During alignment the beam was focused onto the hemisphere centre using a CCD camera and by steering of the lenses in the x and y direction and then aligned to give the required angle of incidence. The collection optics were aligned

using the same silicon peak. An additional camera and lamp allow visual alignments of the sample.

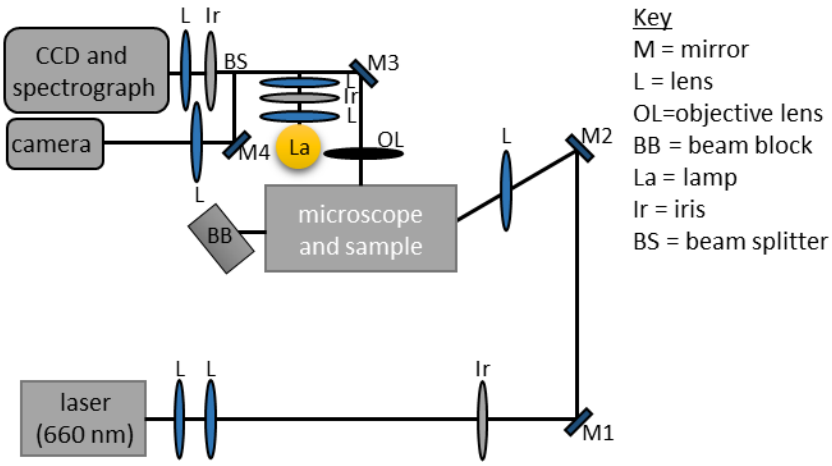

Figure 2.14. Schematic of set-up for System 2 used for TIR Raman spectroscopy. The system was fitted with both a 532 nm and 660 nm laser. The 660 nm was chosen for experimentation in order to reduce fluorescent background signal.

2.2.4.3. System 3: TIR Raman spectroscopy at 660 nm

System 3 (Figure 2.15) was designed and assembled in house and specifically suited this project's requirements, the aim being to give the highest probability of sensing adsorbates at concentrations of monolayer and below during *in situ* catalytic studies. In particular, an Andor Newton 920 BE2X-DD CCD camera was used to enable efficient collection at longer wavelengths, which was found to be a problem using System 2 with the 660 nm excitation source. In design the system is generally similar to System 2. A Laser Quantum gem 660 nm diode laser was used with a laser power of 200 or 800 mW. The beam is expanded to around 9 mm using a telescope and directed to the sample by a series of mirrors. A filter wheel containing a number of different optical density filters was used to reduce the laser power for alignment. The incident beam is then focused on the sample using two cylindrical lenses to enable beam shaping, both placed just before the final alignment mirror. The angle of the incident light was set to approximately 71°. An optional Fresnel Rhomb λ/2 optic can be used on the incident path to rotate the polarisation of the incident light by 90°. A beam block is placed behind (bulk Raman spectroscopy) or after the sample (TIR Raman spectroscopy) to ensure the safe collection of the unabsorbed laser beam. Raman scattered light was then collected using an ultra-long working distance high numerical aperture lens (50X Nikon CFI60 TU Plan Epi ELWD Infinity Corrected Objective, supplied by Edmund Optics). Again an additional camera and lamp allow visual alignments of the sample and are incorporated into the system by insertion or a mirror and a beam splitter

(both installed on flip mounts). A wire grid polariser enables either p or s polarised light to be collected as required. Edge filters are then used to remove the Rayleigh scattered light (two Semrock 664 nm RazorEdge Ultrasteep long-pass edge filters used in series). Finally if the wire grid polariser is being use a depolariser is placed before the slit focusing lens to prevent polarisation dependence of the spectrograph influencing the observed intensity. An Andor Shamrock 303i (fitted with 3 gratings) is then used to disperse light collected onto the CCD above.

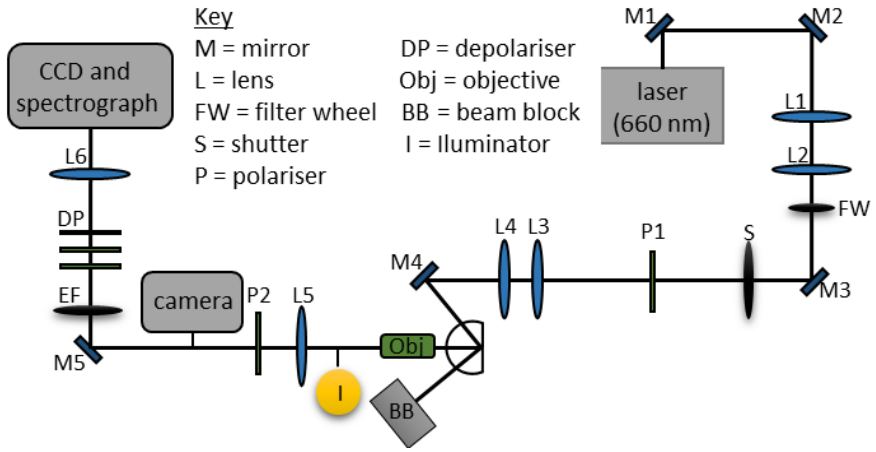

Figure 2.15. Schematic of set-up for System 3 (660 nm) used for TIR Raman spectroscopy. This system was designed and assembled in house specifically to suit our requirements and to give the highest probability of sensing adsorbates at concentrations of monolayer and below during in situ catalytic studies.

The system was calibrated by collecting light from a neon bulb to allow spectral calibration (for wavelength) as well as a white light calibration using a filament lamp as a black-body emitter. The white light calibration was undertaken in order to remove and transmission/throughput the dependence of the overall system (transmission functions of all the collection optics including CCD and spectrograph) from the signal acquired. Due to changes in the focus or the laser power the recorded parts of the spectrum did not necessarily align. Therefore, the overlap between the regions was used to determine a factor by which the intensities varied. This factor was then applied to the whole region in order to align the spectra. At one point the data were cut and the regions put together resulting in a complete aligned spectrum with the intensity at 1000 cm^{-1} considered as true (*i.e.* the intensity in counts s^{-1} of the 1000 cm^{-1} point was the same as in the raw data). Data processing was used for removal of cosmic rays and for the averaging of serval frames of data. A Matlab programme was written for the removal of cosmic rays and Origin was used for smoothing of the averaged data using a Savizky-Golay filter, for which a window of 5 data points was used and plotted. Due to the low sensitivity, of monolayer deposited nanoparticle spectra, these spectra were further processed by division by the clean hemisphere data to

generate a difference spectrum. To this data a background could be fitted to allow further extraction of any spectral features.

Alignment took place at low laser power as described in Chapter 5 working through sequentially from the laser to the CCD. The beam expansion was checked to be 1 cm at both short and long distances from the beam expander. Mirrors M3 and M4 were then used to point and steer the beam, ensuring that the beam went through the centre of the polariser (P1) and the shutter (S). The beam was then aligned onto the hemisphere using lenses L3 and L4, with one focussing in the x and the other in the y direction. Once the laser spot was correctly aligned upon the centre of the flat face of the sample/hemisphere the position can be subtly varied (using L3 and L4) in order to maximise the signal.

2.2.4.4. Bulk and TIR Raman spectroscopy: An overview of the Raman systems used and sample preparation

2.2.4.4.1. TIR Raman spectroscopy

TIR Raman spectroscopy took place on Systems 2 and 3. All TIR Raman samples were prepared by LB trough dipping (Section 2.2.5.9), to give a monolayer sample supported on a silica hemisphere.

2.2.4.4.2. Sample deposition using drop cast method

For deposition using the drop cast methodology nanoparticles dispersed *via* sonication, for a minimum of 10 min in a suitable volatile solvent, were placed drop wise on the surface of the support using a glass pipette. The sample was then left at room temperature for several hours in order to allow for solvent evaporation and thorough drying of the deposited sample.

2.2.4.5. Cell design

For TIR Raman spectroscopy (taking place on Systems 2 and 3) a cell was required to hold the hemisphere securely in place in order to keep the orientation constant to allow for alignment of the laser spot. Two cells were used. A sketch of both cells and the cell holder is given in Figures 2.16 and 2.17. The first (used on System 2 and shown in Figure 2.16 A) was comprised of glass with inlets and outlets allowing for gas flow. In order to allow for heating a second cell was made (stainless steel) (Figure 2.17 B used on both Systems 2 and 3). The clamping of the cell into the holder was subtly changed for the second cell. The first cell had been held in place by two plastic disks clamped together. In order to allow for heating this was replaced

with a metal holder, with the cell held in place using three grub screws.

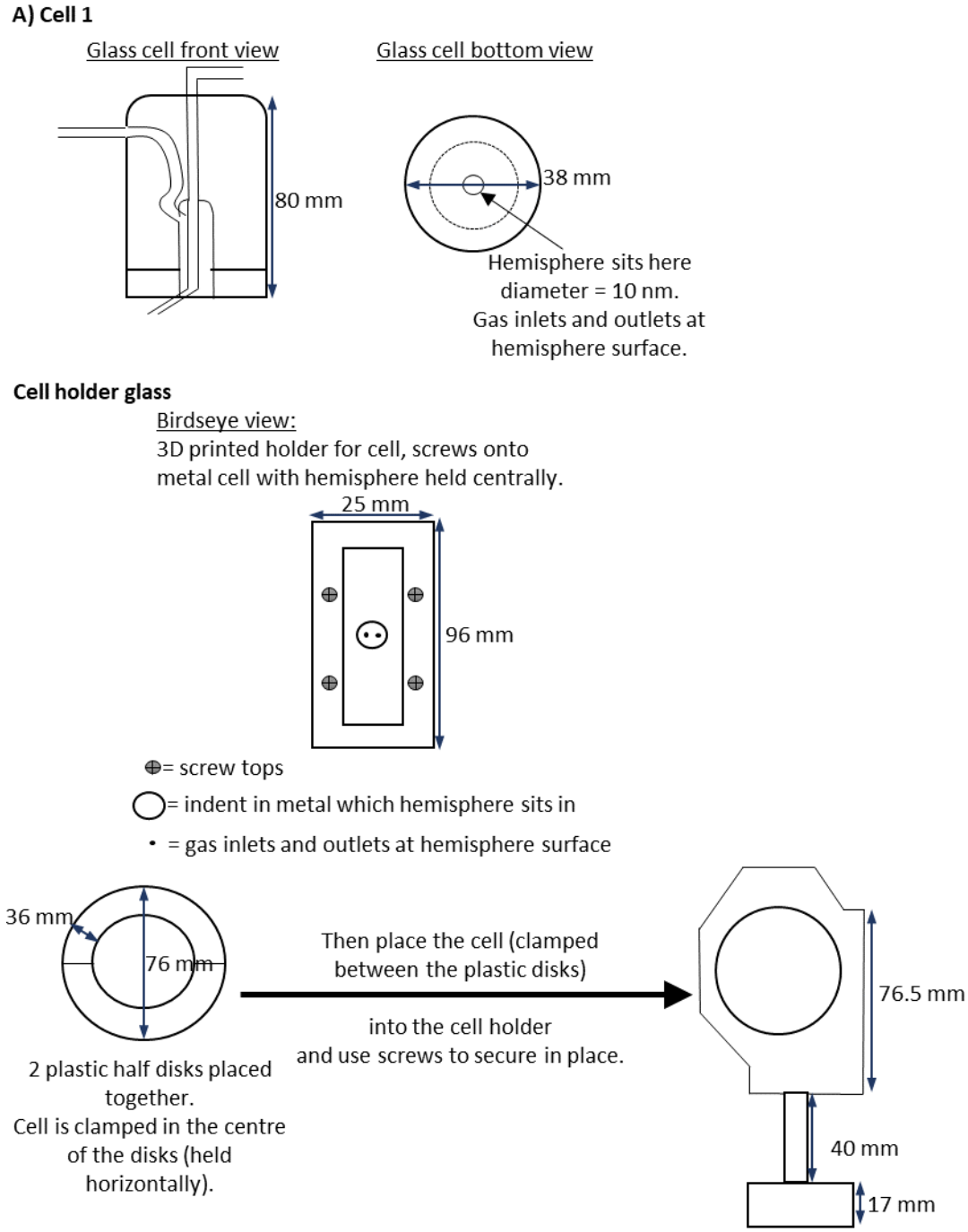

Figure 2.16. Diagram of A) glass cell and holder used for TIR Raman spectroscopy on Systems 2. For the cell and holder the coated hemisphere was held upon the cell base and the cell was then clamped into the holder.

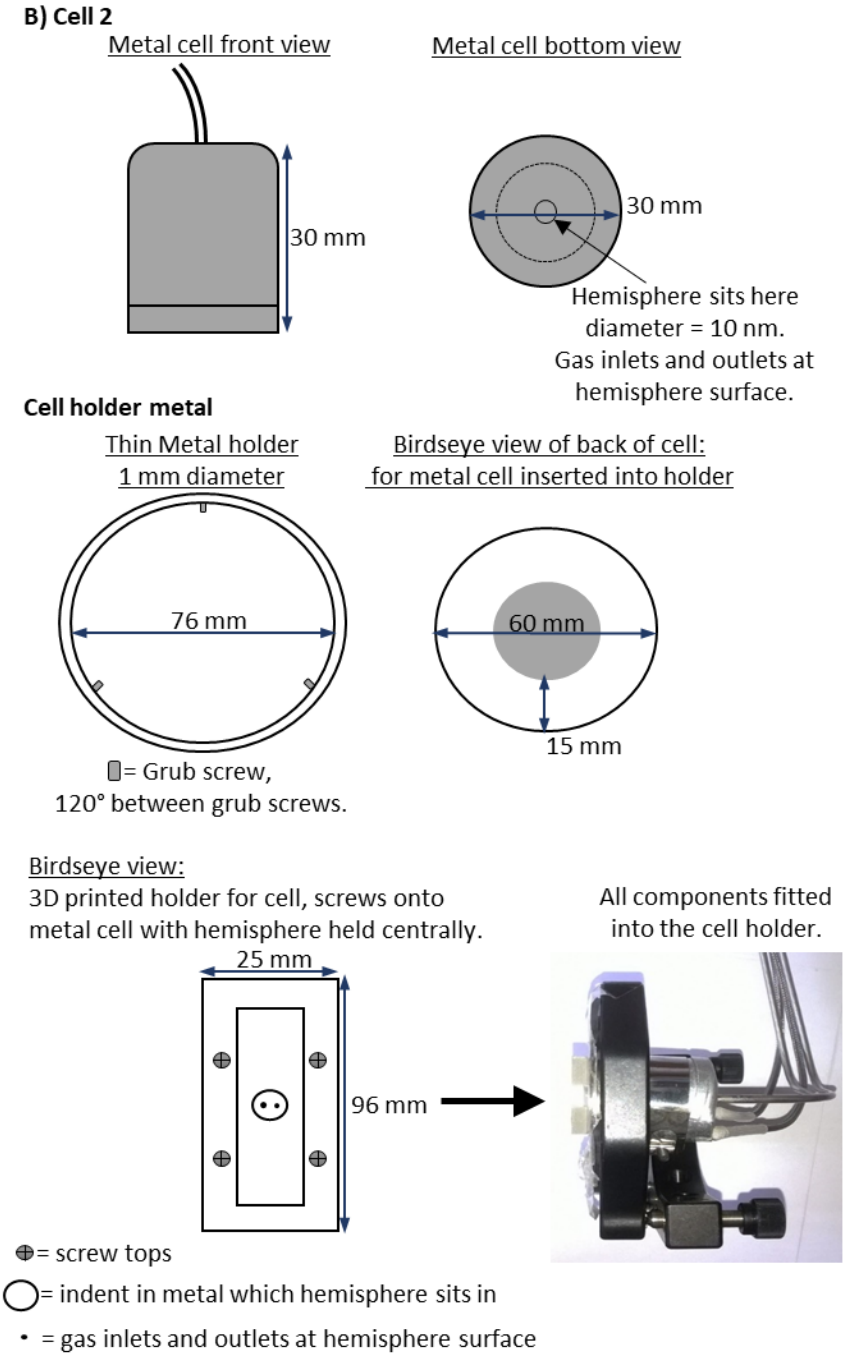

Figure 2.17. Diagram of B) metal cell and holder to allow for heating of the hemisphere used for TIR Raman spectroscopy on Systems 2 and 3. For the cell and holder the coated hemisphere was held upon the cell base and the cell was then clamped into the holder.

2.2.4.6. Plasma cleaning of LB deposited monolayers of nanoparticles upon a silica hemisphere

Plasma cleaning of monolayer coated nanoparticle samples, deposited upon on a silica hemisphere, using LB trough deposition (Section 2.2.5.9) took place using a Bio-rad Polaran Division Plasma Asher E2000, operated using a small air leak flow though the inlet valve and pumped with a rotary pump to generate a low pressure oxygen/nitrogen plasma. Samples were plasma cleaned for varying times, with TIR Raman used to establish cleaning protocols

for organic capping agent removal, with spectra recorded after the cleaning has taken place being free of any features. It was intended that this could allow for the creation of a clean surface, from which catalysis such as ethylene hydrogenation could be followed using TIR Raman. The clean surface or removal of the organic is desired firstly to allow access by reagents and secondly to remove possible overlapping signals from the organic capping species. XPS and SEM were used to confirm that no agglomeration of the metal surface had taken place after the completion of plasma cleaning.

2.2.5. Analytical/ characterisation techniques

2.2.5.1. ^{13}C and ^{1}H, and ^{11}B NMR

Samples were recorded on a Bruker Avance-400 (known locally as b4). All samples were prepared in deuterated chloroform. Typically 40 mg of sample was dissolved in 0.7 mL of deuterated chloroform, and placed in an NMR tube. Sample analysis was carried out using the MestraNova software.

2.2.5.2. IR spectroscopy

Fourier Transform (FT)IR spectroscopy took place for liquid and gel samples. A Perkin Elmer 1600 series FTIR spectrometer, equipped with an ATR accessory was used and 64 scans were recorded. For IR spectroscopy of supernatant solutions, the supernatant was rotary evaporated to remove excess solvent (from the reaction mixture) until a viscous gel was obtained.

2.2.5.3. Gas chromatography – mass spectrometer (GCMS)

GCMS was recorded on a QP2010-Ultra (Shimadzu) GCMS with capabilities for electron ionisation (EI) and chemical ionisation (CI). 1 mg mL^{-1} solutions of sample in dichloromethane were used. For EI for nonpolar compounds a Rxi-5Sil MS column (with dimensions 0.15µm x 10m x 0.15 mm) was used with a temperature programme of 30 °C held for 1 min and then ramped to 300 °C at a rate of 50 °C min^{-1}. For EI for polar compounds a Rxi-17Sil MS column (with dimensions 0.15µm x 10m x 0.15 mm) was used with a temperature programme of 30 °C held for 1 min and then ramped to 300 °C at a rate of 50 °C min^{-1}. For CI for nonpolar compounds a Rxi-5Sil MS column (with dimensions 0.15µm x 10m x 0.15 mm) was used with a temperature programme of 30 °C held for 1 min and then ramped to 250 °C at a rate of 50 °C min^{-1}. For CI for polar compounds a Stabilwax column (with dimensions 0.15µm x 10m x 0.15 mm) was used with a temperature programme of 30 °C held for 1 min and then ramped to 250 °C at a rate of 50 °C min^{-1}. In all cases helium was used as the carrier gas, at a rate of 0.41 mL min^{-1}.

GCMS of oleylamine (Section 3.1.4) was recorded on a *trace GCMS* (Thermo-Finnigan Corporation) in order to allow for variation of the temperature gradient used. For the GC EI MS which took place the GC column has a VF-5MS stationary phase with the dimensions 30 m long, 0.25 mm inner diameter and film thickness 0.25 µm. A carrier gas of 1 mL min^{-1} helium, with a spilt flow of 25 mL min^{-1} was delivered. A GC oven temperature gradient of 40 °C held for 1 min and then ramped to 300 °C at a rate of 10 °C min^{-1}, with a final hold at 300 °C for 20 min used.

2.2.5.4. PXRD

PXRD was recorded on a D8 Advance with a Lynxeye Soller PSD Detector. A copper tube source was used, that produced a mixture of Kα_1 and Kα_2 with a wavelength of 1.5406 Å. The diffractometer was operated in Bragg–Brentano mode with a nickel filter, variable slits and sample changer. The experiment was recorded in the 2θ range from 0.5 to 3 for SBA-15 as directed by relevant literature.[52] No sample preparation was required, for a powdered sample, which was loaded on a plastic puck sample holder.

2.2.5.5. XPS

XPS was conducted on a Kratos Axis Nova instrument. A widescan was recorded for each sample, along with regions of interest, and C 1s used for energy calibration.

Samples for analysis by XPS were prepared by depositing nanoparticles onto a suitable substrate (typically a silicon wafer) using LB deposition techniques (Section 2.2.5.9). Prior to deposition substrates were cleaned by sonication in ethanol and then UHP water.

XP spectra were analysed using Casa XPS as XPS was run at an external facility (Newcastle University). Regions of interest were selected using the quantification function, and a background (typically Shirley) was fitted. The elements function of the software was then used to select the elements present in the region selected. Using the function in the quantification menu the chosen regions (such as silicon and platinum) were integrated for the area under the curve. The element selection made can then be used with the database built into the software to calculate the atomic percentage of the two selected regions, taking into account the relative sensitivities of each of the elements.

2.2.5.6. UV–vis spectroscopy

Spectra were acquired using a Cary 5000 UV-vis-Near Infrared (NIR) machine. Spectra were run in an optically transparent cuvette. The cuvette-solvent spectra was used as a background for the sample spectra.[53] Samples were prepared with a concentration of

1 mg mL^{-1} in a suitable solvent (typically distilled water or ethanol). The concentration could then be adjusted so that spectra gave a suitable value of absorption. This was manipulated using the Beer-Lambert law (Equation 2.11). Where A denotes absorbance (no units), ε the molar extinction coefficient / $dm^3\ mol^{-1}\ cm^{-1}$, c the sample concentration / mol dm^{-3}, and l the path length / cm.

$$A = \varepsilon cl \qquad \textit{Equation 2.11}$$

UV-vis spectra were each recorded three times, and the results were averaged to give a final spectrum.

2.2.5.7. ICP-OES

ICP-OES measurements were then taken on a Horiba Yobin Yvon Ultima2 machine with a sequential monochromator and a radial torch configuration. The instrument was calibrated from 0 mg L^{-1} to 20 mg L^{-1} with standard solutions prepared from 1000 mg L^{-1} stock solutions (Ag BDH SpectrosoL and Cu Fluka TraceCERT) in 2% by volume nitric acid.

Typically samples for ICP-OES were prepared by heating solutions of the sample in a few cm^3 of nitric acid (hydrochloric acid, and aqua regia were also used where indicated) at 80 °C for 1 h. The solutions were then made up to standard concentrations (typically a metal concentration of 10 mg L^{-1}) by dilution in a volumetric flask using UHP water. Supported samples for which the metal was leached from the support were prepared in the same manner except after digestion in acid dilution the sample was centrifuged to remove any remaining support.

2.2.5.8. Nitrogen porosimetry measurements: BET, and BJH analysis

BET and BJH analysis were carried out by Dr Simon Beaumont, recorded using a Micrometrics ASAP 2020 surface area and porosity analyser following degassing at 350 °C in vacuum. The adsorbed gas was nitrogen at liquid nitrogen temperature.

2.2.5.9. LB deposition of nanoparticles

A computer controlled KSV Nima LB trough was used for the nanoparticle deposition. Monolayers of nanoparticles deposited upon a suitable substrate (such as a silicon wafer or silica hemisphere) were prepared by LB deposition. If multiple layers of nanoparticle were required repeated dipping was used. In this case the sample was lowered back down through the solution and then dipped again.

2.2.5.9.1. Sample preparation and substrate cleaning

Before deposition, nanoparticles were precipitated by use of an appropriate antisolvent and centrifugation, before dissolution in the minimum necessary volume of chloroform. A full profile of the surface pressure in the trough as function of barrier position was taken for any new sample batch. Due to the high volatility of chloroform, any sample which has been dispersed in chloroform for some time often required re-dispersing and additional sonication.

Glass and silicon wafers were cleaned prior to deposition by sonication in ethanol for 5 min, then in high purity water for a further 5 min. Finally the wafer was plasma cleaned for 10 min.

Hemispheres were cleaned by sonicating for 10 min in a Nochromix glass cleaning solution, in a PTFE beaker to avoid scratching of the hemisphere. The glass cleaning solution consisted of 1 g of Nochromix in 40 mL of concentrated (>95%) sulfuric acid. The hemisphere was then carefully extracted and sonicated in UHP water. TIR Raman analysis showed this to be an effective cleaning procedure.

2.2.5.9.2. Experimental protocol

The trough (shown in Section 2.1.6, Figure 2.7) was cleaned according to the instruction manual details using ethanol and UHP water. The trough was then assembled and checked to be level (using a spirit level) and the alignment of all components was checked. The trough was then filled with UHP water until water level reached the top of the trough. The trough was then checked to be sufficiently clean by closing the barriers slowly and monitoring that any changes in surface pressure seen did not exceed 0.3 mN m^{-1}, before opening the barriers again and zeroing the surface pressure and barrier positions. The substrate was secured onto the vertical drive. In order to allow hemispheres to be held on the vertical drive a specially designed holder (Figure 2.18) was produced by use of a 3D plastic printer.

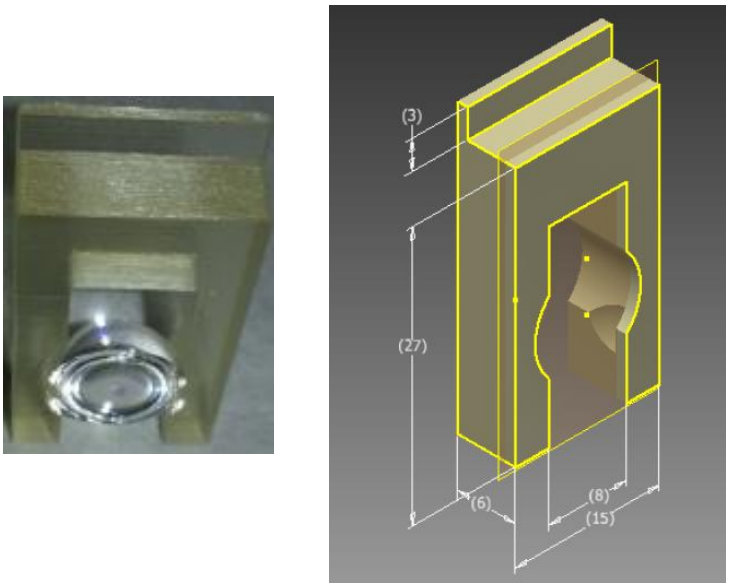

Figure 2.18. Photograph and Computer Aided Design (CAD) drawing of the holder (dimensions in mm) designed to allow a silica hemisphere (diameter 10 mm) to be attached to the vertical drive of a LB trough apparatus. The holder contains two small grooves designed for the hemisphere to fit into so it remains firmly in place during the dipping procedure.

Once the substrate was fitted the vertical drive position was lowered until the substrate just touched the water surface. The vertical drive position was zeroed at this position and the substrate was then fully submerged. The solution to be studied was then pipetted carefully onto the surface of the trough, taking care not to crash the solution through the water surface. The solution was added to the surface until the desired surface pressure was reached or until the surface of the trough appeared fully saturated. The surface pressure was recorded. The trough was then left for 10 min to allow for evaporation of the solvent (chloroform) from the troughs surface. The surface pressure was recorded again. A profile was selected to allow for variation of the surface pressure at the troughs surface, by carefully closing of the barriers at the water surface at a pre-set value (5 mm min^{-1}). The settings typically used are detailed in Table 2.4.

Table 2.4. Typical dipping isotherm settings for LB trough.

Target surface pressure	Depends on nanoparticle and surface packing ≈ 40 mN min^{-1} usual.
Upper limit	10 mm above current vertical drive position.
Speed up	2 mm min^{-1}.
Lower limit	Current vertical drive position.
Speed down	2 mm min^{-1}.

The desired monolayer samples were then prepared by dipping of the substrate. The substrate was held under the water surface in the trough until the desired surface pressure was reached. The substrate was then removed from the trough at a slow controlled rate and the nanoparticle layer adhered to its surface. If required multiple layers could be created by setting the apparatus to slowly place the substrate back into the trough, and remove it again to place a further nanoparticle layer on the substrate. The sample was then left to dry in air, on the jaws of the trough. It should be noted that whether the dipping surface pressure target is achievable will depend on the initial surface pressure of the trough prior to compression of the barriers. A higher initial value will lead to a greater final surface pressure being reached on the trough. Hence if a high dipping surface pressure is required, it may be necessary to place a large amount of nanoparticle on the trough initially. If required optical microscopy could be used to examine the surface of the dipped substrate to check for scratches and macroscopic non-uniformity.

2.2.5.10. TEM

2.2.5.10.1. Microscope details

TEM was conducted on JEOL 2100F FEG TEM at 200 kV, using BF and High Resolution Electron Microscopy (HREM) imaging. The microscope was equipped with a high resolution pole piece giving 2.3 Å point resolution and 1.0 Å information limit. The microscope was also equipped with a Piezo-driven stage for precision sample movement at high magnifications, and a Gatan Orius camera for acquiring high quality images over a wide field of view as well as diffraction patterns. Chemical analysis was performed using EDX analysis, using an Oxford INCAx-sight silicon (lithium) detector for EDX; 50 mm^2 area detector at 25° take off angle providing 130 eV energy resolution. A low background double tilt holder was used for EDX analysis.

2.2.5.10.2. Sample preparation

TEM grids used were supplied by Agar and TAAB and their details were as follows:

Agar S147-3 holey carbon film 300 mesh copper

TAAB C062/C holey carbon film on 3.05 mm diameter 300 mesh copper grid

Agar AGS147N3 holey carbon films on 300 mesh nickel.

Typically solid samples were finely ground by hand, in a pestle and mortar, and the dissolved in an appropriate high purity solvent with sonication. Ethanol (HPLC grade) was typically used as a solvent because it evaporates to dryness completely. Samples which were already in solution were precipitated out with the use of a suitable antisolvent and were then placed in solution with an appropriate high purity solvent *via* sonication. Once in solution sample was pipetted carefully onto a clean TEM grid, the grid was then left to dry, and was stored prior to microscopy in a TEM grid box. Alternatively (where indicated) some nanoparticle TEM samples were prepared directly during LB deposition. The LB trough was used as usual, with the nanoparticle containing phase (in a volatile solvent) added to the trough's surface. A clean TEM grid was then placed on the compressed surface and left for typically 30 seconds. The grid was then carefully removed from the surface, using clean tweezers, and left to dry, before being stored in a TEM grid box prior to imaging. For platinum doped copper nanoparticles the as deposited TEM grid was held under vacuum overnight at 100 °C in a specially designed holder. This allowed for the removal of any excess carbonaceous material that might prohibit the high resolution imaging required.

2.2.5.10.3. Particle size analysis

Particle size analysis was conducted using the programme Image J. Particle size was measured from the diameter of particles relative to the scale bar typically for 100 particles from at least 3 different regions of the holey carbon grid. Particles were measured diagonally to allow for averaging of any perturbation from an exactly spherical particle shape. Particle size for spherical or oval shapes were counted by their typical diameter. Hexagonal shapes (as view in projection) were calculated using their long diameter (perhaps resulting in slightly overestimating their size), but for squares / rectangles (as viewed in projection) a mathematical average of their longest and shortest visible / apparent cross particle lengths was used.

2.2.5.11 SEM

2.2.5.11.1. Microscope details

SEM was performed on an S-5200 Ultra-high Resolution field emission SEM. The microscope was equipped with an ultra-high resolution objective lens, with resolution 1.8 nm at 1 kV or 0.5 nm at 30 kV. A secondary electron (SE) signal detection mode, equipped with a signal control mode, low voltage back-scatter detector mode (BSE), signal mixing mode, YAG BSE mode, and STEM mode was used.

2.2.5.11.2. Sample preparation

Sample for analysis by SEM was prepared by depositing nanoparticle onto a suitable substrate (typically a silicon wafer) using LB deposition techniques (Section 2.2.5.9). Prior to deposition substrates were cleaned by sonication (for a minimum of 10 min) in ethanol and then UHP water. Selected samples supported in this manner were then chromium coated to prevent aggregation of the capping agent upon imaging (Section 3.2.1.3). Plasma cleaning of deposited samples was also undertaken to allow for removal of the capping agent in order to allow SEM to be undertaken (Section 3.6.1.1) and were also studied by SEM (Section 2.2.5.11).

2.2.6. *In situ* studies and catalytic testing

2.2.6.1. Ethylene hydrogenation studied in situ using TIR Raman

Conditions to mimic ethylene hydrogenation were used with the above TIR Raman cell for platinum nanoparticle catalysts (platinum/PVP or platinum/OAm nps) deposited upon a silica hemisphere and plasma cleaned for 2 min for platinum/PVP nps and 1 min for platinum/OAm nps. Experimentation took place on both TIR Raman systems (Systems 2 and 3 see Sections 2.2.4.2 and 2.2.4.3 respectively). Conditions of gas flows used for system 2 and system 3 are given below in Table 2.5 and Table 2.6, respectively. The gas flows were selected based on Cremer *et al*..[40] The gases were delivered to the cell by three gas cylinders (helium CP grade, or nitrogen 99.998% minimum nitrogen, with hydrogen zero grade, and ethylene CP grade) with the gas flow controlled using several MKS GE50A013501AAV010 mass flow controller devices and programmed using LabVIEW. The gas flow rates were calibrated by setting to a specific flow and measuring an atmospheric pressure volume using a bubble flow-meter to give the actual flow in mL min^{-1}. A graph of the mass flow controller input can be plotted against the measured flow. The trend line equation for this graph allows for the calculation of the input required for the mass flow controller in order to achieve the desired actual flow. The gas delivery system comprised 1/8" OD pipe compression fittings (Swagelok or Ham-let)

and was initially *via* a combination of stainless steel and nylon but was replaced entirely by stainless steel in order to allow more readily for cleaning and to prevent leaching of the tubing. The Raman system was vented by connection to the fume hood extraction system.

Table 2.5. Gas flow conditions for ethylene hydrogenation over platinum nanoparticle catalyst (platinum/PVP nps deposited at a monolayer concentration upon a silica hemisphere and plasma cleaned for removal of the capping agent). All TIR Raman took place at 200 mW laser power with 10 acquisitions on system 2 (acquisitions times were varied as stated in Chapter 5, Section 5.1).

Sample	Flow helium / mL min^{-1}	Flow hydrogen / mL min^{-1}	Flow ethylene / mL min^{-1}
Hemisphere	57.4	0	0
Deposited platinum	57.4	9.3	0
Deposited platinum	57.4	9.3	3.3

Table 2.6. Gas flow conditions for ethylene hydrogenation over platinum nanoparticle catalyst (platinum/OAm nps deposited at a monolayer concentration upon a silica hemisphere and plasma cleaned for removal of the capping agent). All TIR Raman took place at 800 mW laser power with 50 acquisitions with a 20 s acquisition time on system 3 as described in Section 5.3).

Sample	Flow helium / mL min^{-1}	Flow hydrogen / mL min^{-1}	Flow ethylene / mL min^{-1}
Hemisphere	5	0	0
Deposited platinum	43	7	0
Deposited platinum	43	7	4
Deposited platinum	0	0	42

2.2.6.2. Silver catalysts for amide bond synthesis

2.2.6.2.1. Synthesis of supported silver catalysts.

Satsuma type catalysts were synthesised by capillary inclusion of silver nitrate upon γ-alumina, as described in Section 2.2.3.3, following the work of Satsuma *et al*..[51] Nanoparticle supported catalysts silver/OAm/OAc nps (ripened for either 2 min or 1 h as described in Section 2.2.1.4) were supported upon γ-alumina using the same methodology (Section

2.2.3.3). A variety of support materials were investigated. A summary of the supported materials synthesised is provided in Table 2.7.

Table 2.7. Summary of silver catalysts synthesised for use in amide bond formation (Section 6.1.1, and 6.1.2). Where Satsuma method refers to catalysts synthesised by capillary inclusion of silver nitrate upon γ-alumina, as described in Section 2.2.3.3, following the work of Satsuma et al.,[51] *and nanoparticle supported catalysts silver/OAm/OAc nps (Ag/OAm/OAc) ripened for either 2 min or 1 h (Section 2.2.1.4) were supported upon γ-alumina, SBA-15, silica gel, or cerium(IV) oxide using the same methodology (Section 2.2.3.3).*

Sample	Support
Satsuma method	γ-alumina
2 min Ag/OAm/OAc	γ-alumina
1 h Ag/OAm/OAc	γ-alumina
2 min Ag/OAm/OAc	SBA-15
1 h Ag/OAm/OAc	silica gel
1 h Ag/OAm/OAc	cerium(IV) oxide

2.2.6.2.2. Calcination and reduction procedures for supported silver catalysts

All supported catalysts were calcined directly after drying (unless otherwise specified) as described in Section 2.2.3.3. In order to provide a catalyst surface with the required oxidation/reduction state the catalyst was then reduced (for a short 10 min period) as indicated in the procedure outlined by Satsuma *et al*..[51] Calcination and reduction of catalysts was carried out in a home-built tube furnace with heating controlled by an omega CN 7500 PID controller and a K-type thermocouple located inside the furnace held with wire against the glass tube in the region containing the sample. Gas flow was controlled by several mass flow controller devices and programmed using Brooks Smart Interface Version 1.0.1.0. The calcination and subsequent reduction conditions used for Satsuma based catalysts (*i.e.* those studied in Section 6.1.1) are summarised below in Table 2.8. For catalysts where it is specified that reduction did not take place the catalyst was calcined (at 600 °C in the manner described in Table 2.8) and then cooled to room temperature for several hours under a 4:1 flow of nitrogen : oxygen. Furthermore for catalysts for which a 3 h reduction period was specified (Section 6.1.1) the gas feed and heating rate conditions within Table 2.8 were followed except that the 10 min reduction period was extended to 3 hours. This was undertaken to

further understand the impact of the short 10 min reduction period (specified by Satsuma *et al*.,[51]) upon the nature of the catalyst surface and the subsequent catalytic behaviour of the material as discussed in Chapter 6.

Table 2.8. Temperature and gas flow conditions for calcination and subsequent reduction of supported silver Satsuma type catalysts for use in amide bond formation reactions (Section 6.1.1).[51] *Where a ramp donates a period in which the temperature is either increased (ramp up) or decreased (ramp down) to a specified value, and a hold donating the time for which the temperature was held (at the temperature specified). Nitrogen was ran through the system prior to and after the flow of the reduction gas mixture (nitrogen : oxygen 50:50) in order to prevent any reaction of the catalyst that might occur if both oxygen and hydrogen gas feeds were present.*

Time- nature of stage	Temperature / °C	Gas flow
3 min-hold	30	nitrogen : oxygen 4:1
1 h-ramp up	600	nitrogen : oxygen 4:1
1 h-hold	600	nitrogen : oxygen 4:1
3 h-ramp down	300	nitrogen : oxygen 4:1 nitrogen only last 15-30 min
10 min-hold	300	nitrogen : oxygen 1:1
2 h-ramp down	20 or room temperature	nitrogen only first 15-30 min, then nitrogen : oxygen 4:1

For the nanoparticle catalysts studied in Section, 6.1.2. Calcination and reduction took place as specified in Table 2.9.

Table 2.9. Temperature and gas flow conditions for calcination and subsequent reduction of supported silver nanoparticle catalysts for use in amide bond formation reactions (Section 6.1.2). Where a ramp donates a period in which the temperature is either increased (ramp up) or decreased (ramp down) to a specified value, and a hold donating the time for which the temperature was held (at the temperature specified). Nitrogen was ran through the system prior to and after the flow of the reduction gas mixture (nitrogen : oxygen 50:50) in order to prevent any reaction of the catalyst that might occur if both oxygen and hydrogen gas feeds were present.

Time- nature of stage	Temperature / °C	Gas flow
3 min- hold	30	argon : oxygen 1:1
27 min-ramp	450	argon : oxygen 1:1
2 h-hold	450	argon : oxygen 1:1
20 min-ramp down	400	argon only
1 h 30 min-hold	400	argon : hydrogen 1:1
30 min-ramp down	30	argon : hydrogen 1:1

Two exceptions to the calcination and reduction procedures described in Table 2.9 are detailed herein. Firstly for silver/OAm/OAc nps supported on ceria the calcination and reduction conditions specified in Table 2.9 were amended to give a temperature of 300 °C for both calcination and reduction. This took place in order to prevent collapse of the mesoporous support as commonly reported in the literature when higher calcination temperatures were employed.[46,47] Secondly for the silver/OAm/OAc nps supported on γ-alumina which are described (within Section 6.1.2) as oxidised only the calcination (at 450 °C under the conditions described in Table 2.9) took place and the sample was then cooled (for 2 h) to room temperature under a 1:1 flow of argon : oxygen.

2.2.6.2.3. Direct dehydrogenative amide synthesis

Once the catalyst had been calcined and reduced (if required) catalytic reaction was undertaken for direct amide bond formation. Two reactions and two different bases were investigated as shown in the Figure 2.19.

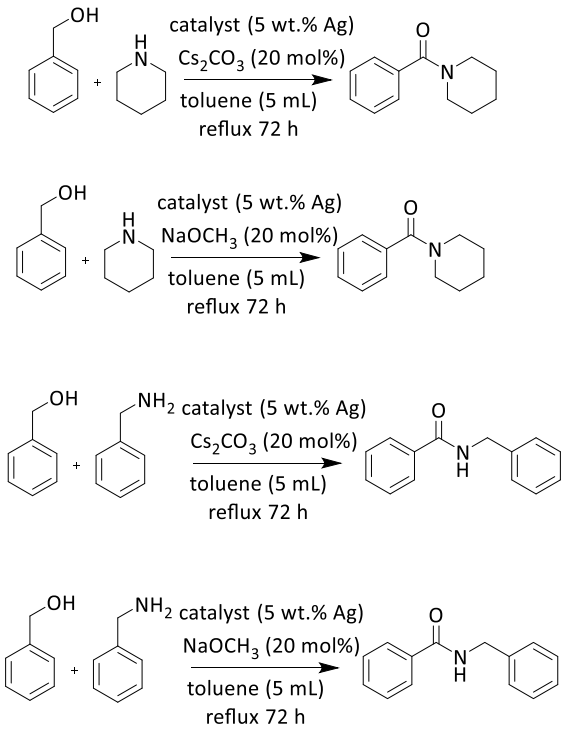

Figure 2.19. Reaction schemes for the two reactions trialled for direct dehydrogenative amide synthesis using two differing bases.

The standard procedure used for catalysis was amended from that reported by Satsuma *et al*.,[51] with the reaction length increased from 24 h to 72 h in order to allow further reaction progress. The amount of solvent was also increased from 2 to 5 mL to ensure effective stirring within the apparatus used.

During a typical reaction either dry caesium carbonate (10 mg, 0.03 mmol) or sodium methoxide (13 mg, 0.2 mmol) (depending upon the reaction being followed) and the silver catalyst being investigated (0.05 g) were added to a Schlenk tube equipped with a condenser, and evacuated and back filled with argon gas. Under argon flow, piperidine (85 mg, 1.0 mmol) and benzyl alcohol (54 mg, 0.5 mmol) or benzylamine (0.11 g, 1.0 mmol) (again dependent upon the reaction being followed) along with the internal standard* were injected into the reaction vessel with 5 mL toluene. With continuous stirring, the system was heated to reflux at 120 °C for three days (72 h) in an oil bath. To stop the reaction, the vessel was rapidly cooled in an ice bath, and subsequently the catalyst was removed by centrifugation at 6000 RPM for 5 min with the liquid phase being decanted. The reaction product was kept in a freezer to ensure no further reaction or side reactions could take place. In order to test numerous catalysts at the same time and, therefore quicken investigations due to the long experimental reaction time, a home built parallel reflux reactor was developed. This enabled a maximum of five reactions to take place at the same time, with

flow of gas and cold water (for the condensers) able to run continuously through the system. The vessel size was 40 mL, and a single reactor is pictured in Figure 2.20. These reactors could be placed on a common hot plate. Stirring was carried out using cross shaped magnetic fleas to maximise stirring efficiency. The hotplate was controlled and the temperature was monitored by use of a temperature probe placed in an additional reactor tube containing a similar volume of oil. It should be noted that for the silver nanoparticle catalyst the same conditions were followed except that the concentration of solvent was doubled. *For the Satsuma type catalyst (Section 6.1.1) methylnaphthalene (71 mg, 0.5 mmol) was added as the internal standard, while for silver nanoparticle catalysts (Section 6.1.2) dodecane was used.

Figure 2.20. Photograph of a single reactor used in the carousel reactor system.

2.2.6.2.4. Analysis of product stream by GC

All reaction products were analysed using GC. The reaction product was further filtered through a pipette packed tightly with filter paper to remove any spent catalyst which remained after centrifugation. As mentioned above internal standards methylnapthalene or dodecane were used to enable the calculation of percentage yield of the amide. GC analysis was carried out using a 5% phenyl/ 95% dimethylpolysiloxane VF-5 ms, 30 min, 0.25 mm, 0.25 µm column. A temperature program of 30 °C for 5 min, 10 °C min^{-1} to 200 °C and hold for 8 min was developed in order to give peak separation for good resolution. The final program had a much longer total time of 30 min compared to initial GC analysis (total program time of 15 min), as the desired product was found to have a very long retention time. Retention times for all reagents and the desired product are shown in Table 2.10. The assignments of retention times in Table 2.10 were made by determining the retention times of genuine samples ran under the same GC conditions for all of the reagents (toluene, methylnaphthalene, dodecane, benzylamine, benzyl alcohol), but for assignment of the

product species GCMS (Section 2.2.5.3) was conducted for the product solution of a reaction, using a similar polarity column. The concentration of each species was calculated, firstly by taking the area under each curve (removing any data points with an area below 0.1 µV min) with each of these areas converted to a percent value of the total area counted under the curves (with exclusion of these small intensity peaks). Response factor calculations were then used in order to allow calculation of product yields as shown in Chapter 6 Appendix.

Table 2.10. GC retention times and assignments for centrifuged and filtered product solutions (for removal of spent catalyst) after direct amide synthesis via the four reactions shown in Figure 2.19. Assignments were made from GCMS of the product solutions and from GC standards for the reagents.

Compound	Retention time / min
Toluene	3.5
Benzylaldehyde	6.5
Benzylamine	9.8
Benzyl alcohol	10.5
Methylnaphthalene	14.1, 14.5
Dodecane	17.5
Benzylidene benzylamide	19.5
Benzoylpiperidine	26.3

2.2.6.3. Platinum doped copper catalysts for furfural hydrogenation

Catalytic testing took place for the copper nanoparticles doped with platinum (Section 2.2.1.7) as well as for the corresponding copper only nanoparticles (Section 2.2.1.5) which were both supported upon alumina at 1 and 2 nominal wt.% of copper respectively (Section 2.2.3.3). All catalysis was performed by collaborators at Aston University. *In situ* reduction and catalysis was carried out in a Hel multi-reactor high pressure platform, housing a bank of 3x 50 mL stainless steel reactor vessels. For each reaction, the catalyst (mass ~30 mg) was heated under flowing hydrogen to 300 °C at a rate of 5 °C min^{-1} and held for 0.5 h. Upon cooling under flowing hydrogen, the autoclaves were sealed and purged with helium to prevent catalyst oxidation. Whilst helium was flowing, the reaction mixture consisting of methanol, (10 mL, Fisher Scientific, 99.99%), furfural (16.5 µL, 0.02 M, Sigma Aldrich), and

decane (38 µL, 0.02 M, Sigma Aldrich) was injected into each reactor. The mixture was allowed to degas for a period of 10 min before pressurising under hydrogen (10 bar, BOC, 99.995%) and heating to 50 °C (stirring at 600 RPM). The reaction was run for 7 h and sampled periodically by slowly depressurizing to atmospheric pressure and then re-pressurizing. Samples were analysed on a Bruker Scion 456-GC equipped with a flame ionization detector and fitted with a Zebron ZB-5 (5%-phenyl-95%-dimethylpolysiloxane) capillary column.

2.2.6.4. Palladium nanoparticles for use in hierarchical structured materials

Platinum and palladium were supported upon bimodal ordered SBA-15 as described in Section 2.2.3.3.1. Catalytic testing was then undertaken by collaborators at Aston University.[54] Catalytic aerobic selective oxidations were performed in a 100 cm^3 Buchi miniclave stirred batch reactor on a 75 cm^3 scale at 150 °C. The catalyst (12.5 mg) was added to reaction mixtures containing 4.2 mmol cinnamyl alcohol (0.562 g), an internal standard (mesitylene, 0.1 cm^3), and toluene solvent (75 cm^3) at 150 °C under 5 bar oxygen and stirring. Reactions were periodically sampled for off-line GC analysis using a Varian 3800GC with an 8400 auto sampler fitted with a CP-Sil5 CB column (15 m × 0.25 mm × 0.25 µm). Conversion, selectivity and yields were calculated through calibration to reference compounds and quoted ±2%. Turnover frequencies for cinnamyl alcohol conversion and cinnamaldehyde production are quoted relative to the surface density of palladium(II) oxide sites (determined by XPS),[55–57] and for cinnamic acid production relative to the surface density of platinum(IV) oxide sites (determined by XPS), these being the respective active sites for selective oxidation over palladium nanoparticles and platinum nanoparticles.

2.3. Bibliography

(1) Reimer, L. *Transmission Electron Microscopy: Physics of Image Formation and Microanalysis*; Springer series in optical sciences; Springer: Berlin, 1984.

(2) Oatley, C. W. *The Scanning Electron Microscope*; Cambridge monographs on physics; Cambridge University Press: London, 1972.

(3) Venezia, A. M. X-Ray Photoelectron Spectroscopy (XPS) for Catalysts Characterization. *Catal. Today* **2003**, *77* (4), 359–370.

(4) Briggs, D. *Surface Analysis of Polymers by XPS and Static SIMS*; Cambridge University Press, 1998.

(5) Fairley, N. *CasaXPS Manual 2.3.15: Introduction to XPS and AES*; Casa Software, Limited, 2009.

(6) Koski, K. J.; Kamp, N. M.; Smith, R. K.; Kunz, M.; Knight, J. K.; Alivisatos, A. P. Structural Distortions in 5–10 Nm Silver Nanoparticles under High Pressure. *Phys. Rev. B* **August 10**, *78* (16), 165410.

(7) Barnes, W. L.; Dereux, A.; Ebbesen, T. W. Surface Plasmon Subwavelength Optics. *Nature* **2003**, *424* (6950), 824–830.

(8) He, R.; Qian, X.; Yin, J.; Zhu, Z. Preparation of Polychrome Silver Nanoparticles in Different Solvents. *J. Mater. Chem.* **2002**, *12* (12), 3783–3786.

(9) Kapoor, S. Preparation, Characterization, and Surface Modification of Silver Particles. *Langmuir* **1998**, *14* (5), 1021–1025.

(10) Link, S.; El-Sayed, M. A. Size and Temperature Dependence of the Plasmon Absorption of Colloidal Gold Nanoparticles. *J. Phys. Chem. B* **1999**, *103* (21), 4212–4217.

(11) Kelly, K. L.; Coronado, E.; Zhao, L. L.; Schatz, G. C. The Optical Properties of Metal Nanoparticles: The Influence of Size, Shape, and Dielectric Environment. *J. Phys. Chem. B* **2003**, *107* (3), 668–677.

(12) Mock, J. J.; Barbic, M.; Smith, D. R.; Schultz, D. A.; Schultz, S. Shape Effects in Plasmon Resonance of Individual Colloidal Silver Nanoparticles. *J. Chem. Phys.* **2002**, *116* (15), 6755–6759.

(13) Mulfinger, L.; Solomon, S. D.; Bahadory, M.; Jeyarajasingam, A. V.; Rutkowsky, S. A.; Boritz, C. Synthesis and Study of Silver Nanoparticles. *J. Chem. Educ.* **2007**, *84* (2), 322.

(14) Eustis, S.; El-Sayed, M. A. Why Gold Nanoparticles Are More Precious than Pretty Gold: Noble Metal Surface Plasmon Resonance and Its Enhancement of the Radiative and Nonradiative Properties of Nanocrystals of Different Shapes. *Chem Soc Rev* **2006**, *35* (3), 209–217.

(15) Liz-Marzán, L. M. Nanometals. *Mater. Today* **2004**, *7* (2), 26–31.

(16) Woods, D. A.; Bain, C. D. Total Internal Reflection Raman Spectroscopy. *Analyst* **2012**, *137* (1), 35–48.

(17) Gardiner, D. J.; Graves, P. R. *Practical Raman Spectroscopy*, Softcover reprint of the original 1st ed. 1989 edition.; Springer: Berlin u.a., 1989.

(18) Ru, E. L.; Etchegoin, P. *Principles of Surface-Enhanced Raman Spectroscopy: And Related Plasmonic Effects*; Elsevier Science: Amsterdam; Boston, 2008.

(19) Atkins, P.; Paula, J. de. *Atkins' Physical Chemistry*, 9 edition.; OUP Oxford: Oxford; New York, 2009.

(20) Wachs, I. E.; Roberts, C. A. Monitoring Surface Metal Oxide Catalytic Active Sites with Raman Spectroscopy. *Chem. Soc. Rev.* **2010**, *39* (12), 5002–5017.

(21) Michaels, C. A. Surface-Sensitive Raman Microscopy with Total Internal Reflection Illumination. *J. Raman Spectrosc.* **2010**, *41* (12), 1670–1677.

(22) Carr, C. W.; Radousky, H. B.; Demos, S. G. Wavelength Dependence of Laser-Induced Damage: Determining the Damage Initiation Mechanisms. *Phys. Rev. Lett.* **2003**, *91* (12).

(23) Bass, M.; Barrett, H. Avalanche Breakdown and the Probabilistic Nature of Laser-Induced Damage. *IEEE J. Quantum Electron.* **1972**, *8* (3), 338–343.

(24) Bain, G. Total Internal Reflection Raman Spectroscopy. Spectroscopy Europe 2004.

(25) Edgepass Filters: Longpass and Shortpass https://www.thorlabs.com/newgrouppage9.cfm?objectgroup_id=918 (accessed Jun 19, 2017).

(26) Mallinson, S. R. Fabry-Perot Interferometer. US4825262 A, April 25, 1989.

(27) Perkampus, H.-H. *Encyclopedia of Spectroscopy*; VCH, 1995.

(28) UV Transmission Gratings https://www.thorlabs.com/newgrouppage9.cfm?objectgroup_id=1122 (accessed Jun 19, 2017).

(29) Zhao, D. Triblock Copolymer Syntheses of Mesoporous Silica with Periodic 50 to 300 Angstrom Pores. *Science* **1998**, *279* (5350), 548–552.

(30) Kleitz, F.; Choi, S. H.; Ryoo, R. Cubic Ia3d Large Mesoporous Silica: Synthesis and Replication to Platinum Nanowires, Carbon Nanorods and Carbon Nanotubes. *Chem. Commun.* **2003**, No. 17, 2136–2137.

(31) Firouzi, A.; Atef, F.; Oertli, A. G.; Stucky, G. D.; Chmelka, B. F. Alkaline Lyotropic Silicate−Surfactant Liquid Crystals. *J. Am. Chem. Soc.* **1997**, *119* (15), 3596–3610.

(32) Hiltrop, K. Lyotropic Liquid Crystals. In *Liquid Crystals*; Topics in Physical Chemistry; Steinkopff, Heidelberg, 1994; pp 143–171.

(33) Alayoglu, S.; An, K.; Melaet, G.; Chen, S.; Bernardi, F.; Wang, L. W.; Lindeman, A. E.; Musselwhite, N.; Guo, J.; Liu, Z.; Marcus, M. A.; Somorjai, G. A. Pt-Mediated Reversible Reduction and Expansion of CeO_2 in Pt Nanoparticle/Mesoporous CeO_2 Catalyst: In Situ X-Ray Spectroscopy and Diffraction Studies under Redox (H_2 and O_2) Atmospheres. *J. Phys. Chem. C* **2013**, *117* (50), 26608–26616.

(34) Tian, B.; Liu, X.; Yang, H.; Xie, S.; Yu, C.; Tu, B.; Zhao, D. General Synthesis of Ordered Crystallized Metal Oxide Nanoarrays Replicated by Microwave-Digested Mesoporous Silica. *Adv. Mater.* **2003**, *15* (16), 1370–1374.

(35) Ren, Y.; Ma, Z.; Qian, L.; Dai, S.; He, H.; Bruce, P. G. Ordered Crystalline Mesoporous Oxides as Catalysts for CO Oxidation. *Catal. Lett.* **2009**, *131* (1–2), 146–154.

(36) Lu, A. H.; Schüth, F. Nanocasting: A Versatile Strategy for Creating Nanostructured Porous Materials. *Adv. Mater.* **2006**, *18* (14), 1793–1805.

(37) Petasch, W.; Kegel, B.; Schmid, H.; Lendenmann, K.; Keller, H. Low-Pressure Plasma Cleaning: A Process for Precision Cleaning Applications. *Surf. Coat. Technol.* **1997**, *97* (1–3), 176–181.

(38) Krier, J. M.; Michalak, W. D.; Baker, L. R.; An, K.; Komvopoulos, K.; Somorjai, G. A. Sum Frequency Generation Vibrational Spectroscopy of Colloidal Platinum Nanoparticle Catalysts: Disordering versus Removal of Organic Capping. *J. Phys. Chem. C* **2012**, *116* (33), 17540–17546.

(39) Mazumder, V.; Sun, S. Oleylamine-Mediated Synthesis of Pd Nanoparticles for Catalytic Formic Acid Oxidation. *J. Am. Chem. Soc.* **2009**, *131* (13), 4588–4589.

(40) Iablokov, V.; Beaumont, S. K.; Alayoglu, S.; Pushkarev, V. V.; Specht, C.; Gao, J.; Alivisatos, A. P.; Kruse, N.; Somorjai, G. A. Size-Controlled Model Co Nanoparticle Catalysts for CO_2 Hydrogenation: Synthesis, Characterization, and Catalytic Reactions. *Nano Lett.* **2012**, *12* (6), 3091–3096.

(41) Mott, D.; Galkowski, J.; Wang, L.; Luo, J.; Zhong, C.-J. Synthesis of Size-Controlled and Shaped Copper Nanoparticles. *Langmuir* **2007**, *23* (10), 5740–5745.

(42) Tao, A.; Kim, F.; Hess, C.; Goldberger, J.; He, R.; Sun, Y.; Xia, Y.; Yang, P. Langmuir−Blodgett Silver Nanowire Monolayers for Molecular Sensing Using Surface-Enhanced Raman Spectroscopy. *Nano Lett.* **2003**, *3* (9), 1229–1233.

(43) Pushkarev, V. V.; An, K.; Alayoglu, S.; Beaumont, S. K.; Somorjai, G. A. Hydrogenation of Benzene and Toluene over Size Controlled Pt/SBA-15 Catalysts: Elucidation of the Pt Particle Size Effect on Reaction Kinetics. *J. Catal.* **8**, *292* (0), 64–72.

(44) Dhainaut, J.; Dacquin, J.-P.; Lee, A. F.; Wilson, K. Hierarchical Macroporous–mesoporous SBA-15 Sulfonic Acid Catalysts for Biodiesel Synthesis. *Green Chem* **2010**, *12* (2), 296–303.

(45) Wainwright, S. G.; Parlett, C. M. A.; Blackley, R. A.; Zhou, W.; Lee, A. F.; Wilson, K.; Bruce, D. W. True Liquid Crystal Templating of SBA-15 with Reduced Microporosity. *Microporous Mesoporous Mater.* **2013**, *172*, 112–117.

(46) Wang, T.; Sel, O.; Djerdj, I.; Smarsly, B. Preparation of a Large Mesoporous CeO_2 with Crystalline Walls Using PMMA Colloidal Crystal Templates. *Colloid Polym. Sci.* **2006**, *285* (1), 1–9.

(47) Lyons, D. M.; Ryan, K. M.; Morris, M. A. Preparation of Ordered Mesoporous Ceria with Enhanced Thermal Stability. *J. Mater. Chem.* **2002**, *12* (4), 1207–1212.

(48) Kleitz, F.; Hei Choi, S.; Ryoo, R. Cubic Ia3d Large Mesoporous Silica: Synthesis and Replication to Platinum Nanowires, Carbon Nanorods and Carbon Nanotubes. *Chem. Commun.* **2003**, No. 17, 2136–2137.

(49) Pirez, C.; Caderon, J.-M.; Dacquin, J.-P.; Lee, A. F.; Wilson, K. Tunable KIT-6 Mesoporous Sulfonic Acid Catalysts for Fatty Acid Esterification. *ACS Catal.* **2012**, *2* (8), 1607–1614.

(50) Alayoglu, S.; Beaumont, S. K.; Melaet, G.; Lindeman, A. E.; Musselwhite, N.; Brooks, C. J.; Marcus, M. A.; Guo, J.; Liu, Z.; Kruse, N.; Somorjai, G. A. Surface Composition Changes of Redox Stabilized Bimetallic CoCu Nanoparticles Supported on Silica under H_2 and O_2 Atmospheres and During Reaction between CO_2 and H_2: In Situ X-Ray Spectroscopic Characterization. *J. Phys. Chem. C* **2013**, *117* (42), 21803–21809.

(51) Shimizu, K.; Ohshima, K.; Satsuma, A. Direct Dehydrogenative Amide Synthesis from Alcohols and Amines Catalyzed by γ-Alumina Supported Silver Cluster. *Chem. - Eur. J.* **2009**, *15* (39), 9977–9980.

(52) Rossinyol, E.; Arbiol, J.; Peiró, F.; Cornet, A.; Morante, J. R.; Tian, B.; Bo, T.; Zhao, D. Nanostructured Metal Oxides Synthesized by Hard Template Method for Gas Sensing Applications. *Sens. Actuators B Chem.* **8**, *109* (1), 57–63.

(53) Shriver, D. F. *Inorganic Chemistry*, 4th ed.; Oxford University Press: Oxford, 2006.

(54) Parlett, C. M. A.; Isaacs, M. A.; Beaumont, S. K.; Bingham, L. M.; Hondow, N. S.; Wilson, K.; Lee, A. F. Spatially Orthogonal Chemical Functionalization of a Hierarchical Pore Network for Catalytic Cascade Reactions. *Nat. Mater.* **2015**, *15* (2), 178–182.

(55) Hackett, S. F. J.; Brydson, R. M.; Gass, M. H.; Harvey, I.; Newman, A. D.; Wilson, K.; Lee, A. F. High-Activity, Single-Site Mesoporous Pd/Al_2O_3 Catalysts for Selective Aerobic Oxidation of Allylic Alcohols. *Angew. Chem.* **2007**, *119* (45), 8747–8750.

(56) Lee, A. F.; Ellis, C. V.; Naughton, J. N.; Newton, M. A.; Parlett, C. M.; Wilson, K. Reaction-Driven Surface Restructuring and Selectivity Control in Allylic Alcohol Catalytic Aerobic Oxidation over Pd. *J. Am. Chem. Soc.* **2011**, *133* (15), 5724–5727.

(57) Durndell, L. J.; Parlett, C. M. A.; Hondow, N. S.; Wilson, K.; Lee, A. F. Tunable Pt Nanocatalysts for the Aerobic Selox of Cinnamyl Alcohol. *Nanoscale* **2013**, *5* (12), 5412.